

Lepton Flavor Violation in the Inert Scalar Model with Higher Representations

Talal Ahmed Chowdhury^a & Salah Nasri^b

^a*Department of Physics, University of Dhaka, P.O. Box 1000, Dhaka, Bangladesh*

^b*Department of Physics, UAE University, P.O. Box 17551, Al-Ain, United Arab Emirates*

E-mail: talal@du.ac.bd, snasri@uaeu.ac.ae

ABSTRACT: We investigate the lepton flavor violation (LFV) in the inert scalar model with higher representations. We generalize the inert doublet model with right handed neutrino by using higher scalar and fermion representation of $SU(2)_L$. As the generalized model and the inert doublet model have the same parameter space, we compare the rates of $\mu \rightarrow e\gamma$, $\mu \rightarrow ee\bar{e}$ and $\mu - e$ conversion in nuclei in the doublet and its immediate extension, the quartet model. We show that the corresponding rates are larger in the case of higher representation compared to the Inert doublet for the same region of parameter space. This implies that such extended models are more constrained by current LFV bounds and will have better prospects in future experiments.

Contents

1	Introduction	2
2	The Model	3
2.1	Mass spectra	5
2.2	Neutrino mass generation	6
2.3	Perturbativity	7
3	Lepton flavor violating processes	8
3.1	$\mu \rightarrow e\gamma$	8
3.2	$\mu \rightarrow ee\bar{e}$	9
3.2.1	γ -penguin contribution	9
3.2.2	Z-penguin contribution	10
3.2.3	Box contribution	11
3.3	$\mu - e$ conversion in nuclei	11
4	Results and Discussion	13
4.1	Constraints and parameter space	13
4.1.1	Collider constraints	13
4.1.2	DM Constraints	13
4.1.3	Gamma ray constraints and Sommerfeld enhancement	15
4.1.4	Scalar coupling and LFV rates with scalar DM	18
4.1.5	Viable parameter space	18
4.2	LFV processes	20
4.2.1	$\text{Br}(\mu \rightarrow e\gamma)$	20
4.2.2	$\text{Br}(\mu \rightarrow ee\bar{e})$	20
4.2.3	$\mu - e$ conversion rate	21
4.2.4	LFV rates in the doublet and quartet	22
5	Conclusions	23
A	Scalar masses	25
A.1	Inert Doublet	25
A.2	Inert Quartet	25
B	Loop functions	26

C	$\mu e \gamma$ vertex, $\mu e Z$ vertex and box diagrams	27
C.1	$\mu e \gamma$ vertex	27
C.2	$\mu e Z$ vertex	27
C.3	Box diagrams	28

1 Introduction

Neutrino oscillation provides the direct evidence for lepton flavor violation in the neutrino sector. Therefore, one also expects LFV in the charged lepton sector which is yet to be observed. This is a generic prediction in most of the neutrino mass models and depending on the realization details of the model, the rates of different LFV processes can be very different. In this paper, we have focused on radiative neutrino mass model at one loop proposed in [1], known as the scotogenic model, where the scalar content of the model is the inert doublet. Apart from its role in neutrino mass generation, the inert doublet has been extensively studied in the context of dark matter [2–9], mirror model and extra generation [10, 11], electroweak phase transition [12–16] and collider studies [17, 18, 21]. As the higher scalar representation is not forbidden by any symmetry in the model, the immediate generalization of the doublet, the quartet with isospin $J = 3/2$ was studied in [22] to check whether it is viable in providing both light scalar dark matter and strong electroweak phase transition in the universe. Here we have incorporated higher scalar representation instead of the doublet in the scotogenic model and determined the viable $SU(2)_L$ fermion multiplet for generating neutrino mass. LFV processes in the scotogenic model with inert doublet has been studied in [23–28] (and references therein). The extension of the scotogenic model has been addressed in [29, 30]. Also larger multiplets have been incorporated in type III seesaw model [31] and in models of radiative neutrino mass generation at higher order with dark matter [32].

The generalization of scotogenic model with higher $SU(2)_L$ half-integer representation does not change the parameter set of the Lagrangian of the inert doublet at the renormalizable level. Therefore it gives us the opportunity to investigate the predictions of LFV processes for different scalar representations for the same region of parameter space. In particular, we compare the LFV processes for the doublet and the quartet in the light of current experimental bounds and future sensitivities.

There have been many great experimental efforts to detect positive LFV signal in $l_\alpha \rightarrow l_\beta \gamma$, $l_\alpha \rightarrow 3l_\beta$ and $\mu - e$ conversion rate in nuclei. In the case of muon radiative decay, the MEG collaboration [33] has put a limit of $\text{Br}(\mu \rightarrow e \gamma) < 5.7 \times 10^{-13}$ [34] and will have sensitivity of 6×10^{-14} after acquiring data for three more years [35]. In addition, current bound on branching ratio of lepton flavor violating 3-body decay, $\mu \rightarrow ee\bar{e}$ is 1×10^{-12} set by SINDRUM experiment [36] and Mu3e experiment

will reach a sensitivity of 10^{-16} [37]. Furthermore, SINDRUM II experiment has put current limit on muon to electron ($\mu - e$) conversion rate in Gold (Au) and Titanium (Ti) nucleus of 7×10^{-13} [38] and 4.3×10^{-12} [39] respectively. The future projects Mu2e [40, 41], DeeMe [42], COMET [43] and PRISM/PRIME [44, 45] will improve this bound from 10^{-14} to 10^{-18} . For other LFV processes and their experimental bounds, please see Table I of [27]. We have compared the predictions of the LFV processes $\mu \rightarrow e\gamma$, $\mu \rightarrow ee\bar{e}$ and $\mu - e$ conversion rate in Au and Ti for both doublet and quartet scalars and our comparison has revealed that the contributions of the quartet in all LFV processes are larger than those of the doublet for the same region of parameter space. Consequently, the contribution of higher scalar representation to LFV processes have better experimental prospects.

The paper is organized as follows. We describe the model in section 2. In section 3 we present the relevant formulas of $\mu \rightarrow e\gamma$, $\mu \rightarrow ee\bar{e}$ and $\mu - e$ conversion processes for the inert doublet and quartet. We present the result in section 4 and conclude in section 5. appendix A contains the mass spectrum of the inert doublet and quartet in our parametrization. The expressions of the loop functions are given in appendix B. In appendix C we collect the Feynman diagrams for $\mu e\gamma$ vertices, μeZ vertices and box diagrams.

2 The Model

Any multiplet charged under $SU(2)_L \times U(1)_Y$ gauge group is characterized by the quantum numbers J and Y , with the electric charge of a component in the multiplet is given by $Q = T_3 + Y$. For half-integer representation $J = n/2$, T_3 ranges from $-\frac{n}{2}$ to $\frac{n}{2}$. So the hypercharge of the multiplet needs to be $Y = \pm T_3$ for one of the components to have neutral charge. For integer representation n , similar condition holds for hypercharge.

The generalized scotogenic model involves one half-integer $SU(2)_L$ scalar multiplet Δ with hypercharge $Y = 1/2$ and three generations of real ($Y = 0$) odd dimensional fermionic multiplets, F_i ($i = 1 - 3$) charged under Z_2 symmetry, $\Delta \rightarrow -\Delta$ and $F_i \rightarrow -F_i$. When the scalar multiplet is fixed to be $J = n/2$, n odd, there are two choices for fermionic multiplet which can give Z_2 even $SU(2)_L \times U(1)_Y$ invariant Yukawa term with the lepton doublet; $J = \frac{n-1}{2}$ or $\frac{n+1}{2}$. The charged lepton sector is augmented by the following terms

$$\mathcal{L} \supset -\frac{M_{F_i}}{2} \overline{F_i^c} P_R F_i + y_{i\alpha} \overline{F_i} \cdot l_\alpha \cdot \Delta + \text{h.c} \quad (2.1)$$

where the dot represents the proper contractions among $SU(2)$ indices. In the subsequent analysis we have chosen fermion multiplet to be $J = \frac{n-1}{2}$.

The general Higgs-scalar multiplet potential, symmetric under Z_2 , can be written in the following form,

$$V_0(\Phi, \Delta) = -\mu^2 \Phi^\dagger \Phi + M_0^2 \Delta^\dagger \Delta + \lambda_1 (\Phi^\dagger \Phi)^2 + \lambda_2 (\Delta^\dagger \Delta)^2 + \lambda_3 |\Delta^\dagger T^a \Delta|^2 + \alpha \Phi^\dagger \Phi \Delta^\dagger \Delta + \beta \Phi^\dagger \tau^a \Phi \Delta^\dagger T^a \Delta + \gamma [(\Phi^T \epsilon \tau^a \Phi)(\Delta^T C T^a \Delta)^\dagger + h.c.] \quad (2.2)$$

Here, τ^a and T^a are the $SU(2)$ generators in fundamental and Δ 's representation respectively. C is an antisymmetric matrix analogous to charge conjugation matrix defined as,

$$C T^a C^{-1} = -T^{aT} \quad (2.3)$$

Since C , is an antisymmetric matrix, it can only be defined for even dimensional space, i.e only for half-integer representation. If the isospin of the representation is J then C is $(2J+1) \times (2J+1)$ dimensional matrix. The generators are normalized in such a way so that they satisfy, for fundamental representation, $Tr[\tau^a \tau^b] = \frac{1}{2} \delta^{ab}$ and for other representations, $Tr(T^a T^b) = D_2(\Delta) \delta^{ab}$. Also $T^a T^a = C_2(\Delta)$. Here, $D_2(\Delta)$ and $C_2(\Delta)$ are Dynkin index and second Casimir invariant for Δ 's representation. Notice that, γ term is only allowed for representation with $(J, Y) = (\frac{n}{2}, \frac{1}{2})$ and it is essential for the generation of neutrino mass at one-loop.

The scalar representation with $(J, Y) = (\frac{n}{2}, \frac{1}{2})$ and the fermionic representation with $(J, Y) = (\frac{n-1}{2}, 0)$ have the component fields denoted as $\Delta^{(Q)}$ and $F^{(Q)}$ respectively where Q is the electric charge. They are written explicitly as

$$\Delta_{\frac{n}{2}} = \begin{pmatrix} \Delta^{(\frac{n+1}{2})} \\ \dots \\ \Delta^{(0)} \equiv \frac{1}{\sqrt{2}}(S + iA) \\ \dots \\ \Delta^{(-\frac{n-1}{2})} \end{pmatrix} \text{ and } \mathbf{F}_{\frac{n-1}{2}} = \begin{pmatrix} F^{(\frac{n-1}{2})} \\ \dots \\ F^{(0)} \\ \dots \\ F^{(-\frac{n+1}{2})} \end{pmatrix} \quad (2.4)$$

For the former representation every component represents a unique field while for the latter there is a redundancy $F^{(-Q)} = (F^{(Q)})^*$.

The choices for real fermion multiplet with the doublet are either $(J, Y) = (0, 0)$ or $(1, 0)$ and with the quartet, choices are either $(J, Y) = (1, 0)$ or $(2, 0)$. Our analysis has focused on the following pairs of scalar and fermionic multiplets: $(\Delta_{J=\frac{1}{2}}, F_{iJ=0})$ and $(\Delta_{J=\frac{3}{2}}, F_{iJ=1})$. In component fields, the doublet scalar D , right handed (RH) neutrino, N_{R_i} and the quartet scalar Δ and the triplet fermion \mathbf{F}_i are expressed as

$$D = \begin{pmatrix} C^+ \\ D^0 \equiv \frac{1}{\sqrt{2}}(S + iA) \end{pmatrix}, N_{R_i}, \Delta = \begin{pmatrix} \Delta^{++} \\ \Delta^+ \\ \Delta^0 \equiv \frac{1}{\sqrt{2}}(S + iA) \\ \Delta'^- \end{pmatrix} \text{ and } \mathbf{F}_i = \begin{pmatrix} F^+ \\ F^0 \\ F^- \end{pmatrix}_i \quad (2.5)$$

2.1 Mass spectra

We now sketch the general form of mass spectrum for the scalar and fermionic multiplet which was also presented in [22]. The neutral component of the scalar multiplet ($Y = 1/2$) will have T_3 eigenvalue as $T_3 = -\frac{1}{2}$. Now for the Higgs vacuum expectation value, $\langle \Phi \rangle = (0, \frac{v}{\sqrt{2}})^T$, the term $\langle \Phi^\dagger \rangle \tau^3 \langle \Phi \rangle$ gives $-\frac{v^2}{4}$. So masses for the neutral components, S and A are splitted by the γ term as

$$m_S^2 = M_0^2 + \frac{1}{2} \left(\alpha + \frac{1}{4} \beta + p(-1)^{p+1} \gamma \right) v^2 \quad (2.6)$$

$$m_A^2 = M_0^2 + \frac{1}{2} \left(\alpha + \frac{1}{4} \beta - p(-1)^{p+1} \gamma \right) v^2 \quad (2.7)$$

Here, $p = \frac{1}{2} \text{Dim}(\frac{n}{2}) = 1, 2, \dots$ comes from $2p \times 2p$ C matrix. For the charged component, with $T_3 = m$, where, $m = n/2, n/2 - 1, \dots, -n/2$, we have,

$$m_{(m)}^2 = M_0^2 + \frac{1}{2} \left(\alpha - \frac{1}{2} \beta m \right) v^2. \quad (2.8)$$

Moreover, because of the γ term, there will be mixing between components carrying same amount of charge. A component of the multiplet is denoted as $|J, T_3\rangle$. Components with $|\frac{n}{2}, m\rangle$ and $|\frac{n}{2}, -(m+1)\rangle$ (such that $-m-1 \geq -\frac{n}{2}$) will have positive and negative charge $Q = m + \frac{1}{2}$ respectively. Now $\langle \Phi \rangle^T \epsilon \tau^a \langle \Phi \rangle$ gives $\frac{v^2}{2\sqrt{2}}$. Therefore, the mixing matrix between components with charge $|Q|$ is,

$$M_Q^2 = \begin{pmatrix} m_{(m)}^2 & \frac{\gamma v^2}{4} \sqrt{\left(\frac{n}{2} - m\right) \left(\frac{n}{2} + m + 1\right)} \\ \frac{\gamma v^2}{4} \sqrt{\left(\frac{n}{2} - m\right) \left(\frac{n}{2} + m + 1\right)} & m_{(-m-1)}^2 \end{pmatrix} \quad (2.9)$$

And the mass eigenstates are,

$$\begin{aligned} \Delta_1'^Q &= \cos \theta_Q \Delta_{(m)}^Q + \sin \theta_Q \Delta_{(-m-1)}^{*Q} \\ \Delta_2'^Q &= -\sin \theta_Q \Delta_{(m)}^Q + \cos \theta_Q \Delta_{(-m-1)}^{*Q} \end{aligned} \quad (2.10)$$

where we have

$$\tan 2\theta_Q = \frac{2(M_Q^2)_{12}}{(M_Q^2)_{11} - (M_Q^2)_{22}} \quad (2.11)$$

Note that the real fermionic multiplet is degenerate at the tree level. However, there is a small splitting between the charged and neutral component due to radiative correction which is $O(100 \text{ MeV})$ [46]. This splitting is needed in order to treat the neutral fermion as the dark matter candidate.

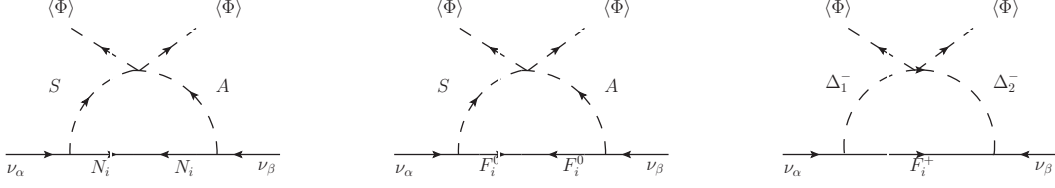


Figure 1. Neutrino mass generation in the inert doublet (first figure from the left) and the quartet (second and third figures).

2.2 Neutrino mass generation

The light neutrino masses are generated at one-loop level as shown in figure 1. The neutrino mass matrix is expressed as

$$\begin{aligned}
 (m_\nu)_{\alpha\beta} &= \sum_{i=1}^3 \frac{y_{\alpha i} y_{i\beta} M_{F_i}}{16\pi^2} \left\{ C_{\frac{1}{2},0,-\frac{1}{2}}^2 \left[\frac{m_S^2}{m_S^2 - m_{F_i}^2} \ln \frac{m_S^2}{m_{F_i}^2} - \frac{m_A^2}{m_A^2 - m_{F_i}^2} \ln \frac{m_A^2}{m_{F_i}^2} \right] \right. \\
 &\quad \left. + \sum_{Q \neq 0} C_{\frac{1}{2},m+\frac{1}{2},m} C_{\frac{1}{2},-m-\frac{1}{2},-m-1} R_{1,m} R_{2,-m-1} \left[\frac{m_{Q,1}^2}{m_{Q,1}^2 - m_{F_i}^2} \ln \frac{m_{Q,1}^2}{m_{F_i}^2} - \frac{m_{Q,2}^2}{m_{Q,2}^2 - m_{F_i}^2} \ln \frac{m_{Q,2}^2}{m_{F_i}^2} \right] \right\} \\
 &= (y^T \Lambda y)_{\alpha\beta}
 \end{aligned} \tag{2.12}$$

Here C_{m_1, m_2, m_3} is the Clebsh-Gordon (CG) coefficient and m_1 , m_2 and m_3 are the T_3 eigenvalues of lepton doublet, fermion and scalar multiplet respectively. Non-zero CG coefficient requires $m_1 + m_3 = m_2$. Also $R_{i,m}$ is the element of the rotation matrix that mixes the two scalar components with same charge $|Q|$ and $m_{Q,i}^2$ are the corresponding mass eigenvalues. Moreover, Λ_i is the loop function,

$$\begin{aligned}
 \Lambda_i &= \frac{M_{F_i}}{16\pi^2} \left\{ C_{\frac{1}{2},0,-\frac{1}{2}}^2 \left[\frac{m_S^2}{m_S^2 - m_{F_i}^2} \ln \frac{m_S^2}{m_{F_i}^2} - \frac{m_A^2}{m_A^2 - m_{F_i}^2} \ln \frac{m_A^2}{m_{F_i}^2} \right] + \sum_{Q \neq 0} C_{\frac{1}{2},m+\frac{1}{2},m} C_{\frac{1}{2},-m-\frac{1}{2},-m-1} \right. \\
 &\quad \left. R_{1,m} R_{2,-m-1} \left[\frac{m_{Q,1}^2}{m_{Q,1}^2 - m_{F_i}^2} \ln \frac{m_{Q,1}^2}{m_{F_i}^2} - \frac{m_{Q,2}^2}{m_{Q,2}^2 - m_{F_i}^2} \ln \frac{m_{Q,2}^2}{m_{F_i}^2} \right] \right\}
 \end{aligned} \tag{2.13}$$

Therefore the neutrino mass at one loop in the doublet case is given by

$$(m_\nu)_{\alpha\beta}^{\text{doublet}} = \sum_{i=1}^3 \frac{y_{\alpha i} y_{i\beta} M_{N_i}}{16\pi^2} \left[\frac{m_S^2}{m_S^2 - m_{N_i}^2} \ln \frac{m_S^2}{m_{N_i}^2} - \frac{m_A^2}{m_A^2 - m_{N_i}^2} \ln \frac{m_A^2}{m_{N_i}^2} \right] \tag{2.14}$$

where M_{N_i} is the mass of the i -th right handed neutrino. When $m_S^2 \sim m_A^2 \equiv m_0^2$ then eq. (2.14) gets simplified

$$(m_\nu)_{\alpha\beta}^{\text{doublet}} = \sum_{i=1}^3 \frac{y_{\alpha i} y_{i\beta} \gamma v^2}{16\pi^2 M_{N_i}} \left[\frac{m_{N_i}^2}{m_0^2 - m_{N_i}^2} + \left(\frac{m_{N_i}^2}{m_0^2 - m_{N_i}^2} \right)^2 \ln \frac{m_{N_i}^2}{m_0^2} \right] \tag{2.15}$$

On the other hand, the neutrino mass matrix in the quartet case is given by

$$(M_\nu)_{\alpha\beta}^{\text{quartet}} = \sum_{i=1}^2 y_{\alpha i} \Lambda_i y_{i\beta} \quad (2.16)$$

with the loop factor,

$$\begin{aligned} \Lambda_i^{\text{quartet}} = & \frac{1}{3(4\pi)^2} M_{Fi} \left[\frac{m_S^2}{m_S^2 - M_{Fi}^2} \ln \frac{m_S^2}{M_{Fi}^2} - \frac{m_A^2}{m_A^2 - M_{Fi}^2} \ln \frac{m_A^2}{M_{Fi}^2} \right] \\ & + \frac{1}{6(4\pi)^2} \sin 2\theta M_{Fi} \left[\frac{m_{\Delta_1^+}^2}{m_{\Delta_1^+}^2 - M_{Fi}^2} \ln \frac{m_{\Delta_1^+}^2}{M_{Fi}^2} - \frac{m_{\Delta_2^+}^2}{m_{\Delta_2^+}^2 - M_{Fi}^2} \ln \frac{m_{\Delta_2^+}^2}{M_{Fi}^2} \right] \end{aligned} \quad (2.17)$$

Explicit expressions of masses in the inert doublet and quartet models are included in appendix A.

The neutrino mass matrix can be diagonalized as

$$U_{PMNS}^T m_\nu U_{PMNS} \equiv \hat{m}_\nu \quad (2.18)$$

where

$$U_{PMNS} = \begin{pmatrix} c_{12}c_{13} & s_{12}c_{13} & s_{13}e^{i\delta} \\ -s_{12}c_{23} - c_{12}s_{23}s_{13}e^{-i\delta} & c_{12}c_{23} - s_{12}s_{23}s_{13}e^{-i\delta} & s_{23}c_{13} \\ s_{12}s_{23} - c_{12}c_{23}s_{13}e^{-i\delta} & -c_{12}s_{23} - s_{12}c_{23}s_{13}e^{-i\delta} & c_{23}c_{13} \end{pmatrix} \times \begin{pmatrix} 1 & 0 & 0 \\ 0 & e^{i\alpha/2} & 0 \\ 0 & 0 & e^{i\beta/2} \end{pmatrix} \quad (2.19)$$

Here, $c_{ij} = \cos \theta_{ij}$, $s_{ij} = \sin \theta_{ij}$, δ is the Dirac phase and α, β are the Majorana phases.

The Yukawa matrix $y_{i\alpha}$ ($\alpha = e, \mu, \tau$) is expressed using the Casas-Ibarra parametrization [49] so that the chosen parameter space automatically satisfies the low energy neutrino parameters,

$$y = \sqrt{\Lambda}^{-1} R \sqrt{\hat{m}_\nu} U_{PMNS}^\dagger \quad (2.20)$$

where R is a complex orthogonal matrix.

2.3 Perturbativity

If there are N generations of right handed fermion multiplet, perturbativity of the Yukawa gives the following constraint [50, 51]

$$\text{Tr}(y^\dagger y) = \sum_{i=1}^3 \sum_{j=1}^N |R_{ij}|^2 \frac{\hat{m}_{\nu_i}}{\Lambda_j} \lesssim O(1) \quad (2.21)$$

If R is taken to be real, the constraint translates into the largest ratio, $\frac{\hat{m}_{\nu_i}}{\Lambda_j} \lesssim O(1)$, whereas for the general case when R is complex, each entry will be bounded as $|R_{ij}| \lesssim \sqrt{\frac{\Lambda_j}{3N\hat{m}_{\nu_i}}}$.

3 Lepton flavor violating processes

In this section we have presented the relevant analytical formulas of LFV processes for the doublet and quartet case. In the standard model due to the GIM suppression the rate of $\mu \rightarrow e\gamma$ becomes $\sim 10^{-54}$ thus negligible. On the other hand the presence of heavy right handed neutrino that mixes with left handed (LH) neutrinos, spoils the GIM suppression and one could obtain the rate which can be probed by experiment [52–58]. In inert scalar models, Z_2 symmetry forbids the mixing between LH and RH neutrinos but the enhancements in the LFV processes are provided by the $C^\pm - N_{R_i}$ loops in the doublet and $\Delta - F_i$ loops in the quartet model. We have focused on three LFV processes: $\mu \rightarrow e\gamma$, $\mu \rightarrow ee\bar{e}$ and $\mu - e$ conversion in nuclei in this paper as they have the most stringent limits from the experiments.

3.1 $\mu \rightarrow e\gamma$

The branching ratio for $\mu \rightarrow e\gamma$, normalized by $\text{Br}(\mu \rightarrow e\bar{\nu}_e\nu_\mu)$, is [27, 59]

$$\text{Br}(\mu \rightarrow e\gamma) = \frac{3(4\pi)^3\alpha_{em}}{4G_F^2}|A_D|^2 \text{Br}(\mu \rightarrow e\nu_\mu\bar{\nu}_e) \quad (3.1)$$

where A_D is the dipole form factor. The Feynman diagrams of one-loop contributions by the doublet and quartet to the $\mu e\gamma$ vertex that enters into the dipole form factor calculation, are given in figure 9.

The contributions from the doublet is the following,

$$A_D^{\text{doublet}} = \sum_{i=1}^3 \frac{y_{ei}^* y_{i\mu}}{32\pi^2} \frac{1}{m_C^2} F^{(n)}(x_{i\sigma}) \quad (3.2)$$

Here $F^{(n)}(x)$ is the loop function given in the appendix B and $x_{i\sigma} = m_{N_i}^2/m_\sigma^2$, where $\sigma = C^+$. On the other hand, the quartet contribution will have two parts

$$A_D^{\text{quartet}} = A_{D(n)}^{\text{quartet}} + A_{D(c)}^{\text{quartet}} \quad (3.3)$$

where $A_{D(n)}^{\text{quartet}}$ is the contribution of the neutral component and $A_{D(c)}^{\text{quartet}}$ is that of the charged component of the fermion triplet. Also, for the notational convenience, we introduce generalized Yukawa coupling $y_{i\alpha\sigma} = y_{i\alpha} C_\sigma$ where C_σ is the corresponding Clebsh Gordon coefficient associated with σ -th component of the quartet. The two contributions are

$$A_{D(n)}^{\text{quartet}} = \sum_{i=1}^3 \sum_{\sigma} \frac{y_{ei\sigma}^* y_{i\mu\sigma}}{32\pi^2} \frac{1}{m_\sigma^2} F^{(n)}(x_{i\sigma}) \quad (3.4)$$

where $x_{i\sigma} = m_{F_i^0}^2/m_\sigma^2$, $\sigma = \Delta_1^+, \Delta_2^+$. And

$$A_{D(c)}^{\text{quartet}} = - \sum_{i=1}^3 \sum_{\sigma} \frac{y_{ei\sigma}^* y_{i\mu\sigma}}{32\pi^2} \frac{1}{m_\sigma^2} F^{(c)}(x_{i\sigma}) \quad (3.5)$$

where $x_{i\sigma} = m_{F_i^\pm}^2/m_\sigma^2$, and $\sigma = \Delta^{++}, S, A$.

3.2 $\mu \rightarrow ee\bar{e}$

Now we turn to $\mu \rightarrow ee\bar{e}$ decay. The branching ratio is given as [27, 59, 60]

$$\begin{aligned} \text{Br}(\mu \rightarrow ee\bar{e}) = & \frac{3(4\pi)^2 \alpha_{em}^2}{8G_F^2} \left[|A_{ND}|^2 + |A_D|^2 \left(\frac{16}{3} \ln \frac{m_\mu}{m_e} - \frac{22}{3} \right) + \frac{1}{6} |B|^2 \right. \\ & \left. + \frac{1}{3} (2|F_Z^L|^2 + |F_Z^R|^2) + \left(-2A_{ND}A_D^* + \frac{1}{3}A_{ND}B^* - \frac{2}{3}A_DB^* + \text{h.c} \right) \right] \\ & \times \text{Br}(\mu \rightarrow e\bar{\nu}_e\nu_\mu) \end{aligned} \quad (3.6)$$

where A_D and A_{ND} are the dipole and non-dipole contribution from the photonic penguin diagrams respectively. Also B represents the contribution from the box diagrams. Moreover, F_Z^L and F_Z^R are given as

$$F_Z^L = \frac{F_Z g_L^l}{g^2 m_Z^2 \sin^2 \theta_W}, \quad F_Z^R = \frac{F_Z g_R^l}{g^2 m_Z^2 \sin^2 \theta_W} \quad (3.7)$$

Here, F_Z is the Z-penguin contribution and g_L^l and g_R^l are the Z-boson coupling to the LH and RH charged leptons respectively. In this model, Higgs penguin contribution will be suppressed by the small electron Yukawa coupling, and therefore we have only considered the photon penguin, Z-boson penguin and box diagrams.

3.2.1 γ -penguin contribution

First let us consider contributions from the photon penguin diagrams. In this case the γ line of $\mu e \gamma$ vertex given in figure 9 will have $\bar{e}e$ attached to it. The photonic non-dipole contribution, A_{ND} for the doublet is in the following

$$A_{ND}^{\text{doublet}} = \sum_{i=1}^3 \frac{y_{ei}^* y_{i\mu}}{96\pi^2} \frac{1}{m_C^2} G^{(n)}(x_{i\sigma}) \quad (3.8)$$

The photonic non-dipole contribution, for the case of the quartet, will again have two parts,

$$A_{ND}^{\text{quartet}} = A_{ND(n)}^{\text{quartet}} + A_{ND(c)}^{\text{quartet}} \quad (3.9)$$

Here $A_{ND(n)}^{\text{quartet}}$ is the contribution of the neutral component and $A_{ND(c)}^{\text{quartet}}$ is the contribution of the charged component of the fermion triplet.

$$A_{ND(n)}^{\text{quartet}} = \sum_{i=1}^3 \sum_{\sigma=\Delta_1^+, \Delta_2^+} \frac{y_{ei\sigma}^* y_{i\mu\sigma}}{96\pi^2} \frac{1}{m_\sigma^2} G^{(n)}(x_{i\sigma}) \quad (3.10)$$

where again $x_{i\sigma} = m_{F_i^0}^2/m_\sigma^2$. And the charged component of fermion triplet contributes as follows,

$$A_{ND(c)}^{\text{quartet}} = - \sum_{i=1}^3 \sum_{\sigma} \frac{y_{ei\sigma}^* y_{i\mu\sigma}}{96\pi^2} \frac{1}{m_\sigma^2} G^{(c)}(x_{i\sigma}) \quad (3.11)$$

with $x_{i\sigma} = m_{F_i^\pm}^2/m_\sigma^2$, and $\sigma = \Delta^{++}, S, A$. The loop functions $F^{(n)}(x)$, $F^{(c)}(x)$, $G^{(n)}(x)$ and $G^{(c)}(x)$ are given in the appendix B.

3.2.2 Z-penguin contribution

Now we focus on the Z-penguin diagram. The Feynman diagrams of one-loop contributions from the doublet and the quartet to the $\mu e Z$ vertex are presented in figure 10. In Z-penguin diagram, the Z line of $\mu e Z$ vertex will have $\bar{e}e$ line attached to it. For the doublet, the contribution is given by the neutral fermion. Following the formulas given in [60, 62, 63]¹

$$F_{Z(n)}^{\text{doublet}} = -\frac{1}{16\pi^2} \sum_{i=1}^3 y_{ei}^* y_{i\mu} \left[2 g_{ZC^+C^-} C_{24}(m_{N_i}, m_C, m_C) + g_L^l B_1(m_{N_i}, m_C) \right] \quad (3.12)$$

Here, $g_{ZC^+C^-}$ is the Z boson coupling to C^\pm of the doublet and g_L^l is the Z boson coupling to LH charged leptons given by

$$g_L^l = \frac{g}{\cos \theta_W} \left(-\frac{1}{2} + \sin^2 \theta_W \right) \quad (3.13)$$

On the other hand, the quartet contribution is

$$F_Z^{\text{quartet}} = F_{Z(n)}^{\text{quartet}} + F_{Z(c)}^{\text{quartet}} \quad (3.14)$$

where the neutral fermion of the triplet contributes as

$$F_{Z(n)}^{\text{quartet}} = -\frac{1}{16\pi^2} \sum_{i=1}^3 \sum_{\sigma_1, \sigma_2} \left[2 y_{ei\sigma_1}^* y_{i\mu\sigma_2} g_{Z\sigma_1\sigma_2} C_{24}(m_{F_i^0}, m_{\sigma_1}, m_{\sigma_2}) + y_{ei\sigma_1}^* y_{i\mu\sigma_1} g_L^l B_1(m_{F_i^0}, m_{\sigma_1}) \right] \quad (3.15)$$

where $\sigma_{1,2} \in \{\Delta_1^+, \Delta_2^+\}$ and $g_{Z\sigma_1\sigma_2}$ is the Z boson coupling to σ_1 and σ_2 scalars of the quartet. The charged fermion of the triplet has the following contribution

$$F_{Z(c)}^{\text{quartet}} = -\frac{1}{16\pi^2} \sum_{i=1}^3 \sum_{\sigma_1, \sigma_2} \left\{ y_{ei\sigma_1}^* y_{i\mu\sigma_1} g_{ZF_i^\pm \overline{F_i^\pm}} \left[\left(2C_{24}(m_{\sigma_1}, m_{F_i^\pm}, m_{F_i^\pm}) + \frac{1}{2} \right) + m_{F_i^\pm}^2 C_0(m_{\sigma_1}, m_{F_i^\pm}, m_{F_i^\pm}) \right] + 2 y_{ei\sigma_1}^* y_{i\mu\sigma_2} g_{Z\sigma_1\sigma_2} C_{24}(m_{F_i^\pm}, m_{\sigma_1}, m_{\sigma_2}) + y_{ei\sigma_1}^* y_{i\mu\sigma_1} g_L^l B_1(m_{F_i^\pm}, m_{\sigma_1}) \right\} \quad (3.16)$$

Here σ_1 and σ_2 range over the S , A , Δ^{++} , and $g_{ZF_i^\pm \overline{F_i^\pm}}$ is the coupling of Z boson to charged fermions. Moreover, B_1 , C_0 and C_{24} are the loop functions, adopted from [60, 62, 63], presented in the appendix B. As B_1 and C_{24} arise from divergent loop integrals, for large M ,

$$C_{24}(M, m, m) \rightarrow \frac{1}{4} \ln \frac{M^2}{\mu^2}, \quad B_1 \rightarrow \frac{1}{2} \ln \frac{M^2}{\mu^2} \quad (3.17)$$

¹[60] contained a mistake in the calculation of Z-penguin diagram which was pointed out in [61]. Subsequently, correct results were presented in [62] and [63]. Moreover, C_{00} of [62] and C_{24} of [63] only differ by an overall minus sign.

Therefore the combination $2xC_{24} + yB_1$ in Z-penguin contribution eq. (3.15) or in eq. (3.16) is vanishing at very large mass M when there are specific relations set by group theoretical requirements in vertex factors x and y .

3.2.3 Box contribution

Lastly the box contribution for the doublet case, presented in figure 11, is [60]

$$e^2 B_{(n)}^{\text{doublet}} = \frac{1}{16\pi^2} \sum_{i,j=1}^3 \left[\frac{\tilde{D}_0}{2} y_{ei}^* y_{i\mu} y_{ej}^* y_{je} + D_0 m_{N_i} m_{N_j} y_{ei}^* y_{ei}^* y_{j\mu} y_{je} \right] \quad (3.18)$$

where, $\tilde{D}_0 = \tilde{D}_0(m_{N_i}, m_{N_j}, m_C, m_C)$ and $D_0 = D_0(m_{N_i}, m_{N_j}, m_C, m_C)$ are loop functions given in the appendix B.

For the quartet case, the contribution of the box diagram can be written as

$$B^{\text{quartet}} = B_{(n)}^{\text{quartet}} + B_{(c)}^{\text{quartet}} \quad (3.19)$$

with $B_{(n)}^{\text{quartet}}$ is the contribution due to the neutral fermions and it is given by

$$e^2 B_{(n)}^{\text{quartet}} = \frac{1}{16\pi^2} \sum_{i,j=1}^3 \sum_{\sigma_1, \sigma_2} \left[\frac{\tilde{D}_0}{2} y_{ei\sigma_1}^* y_{i\mu\sigma_2} y_{ej\sigma_2}^* y_{je\sigma_1} + D_0 m_{F_i^0} m_{F_j^0} y_{ei\sigma_1}^* y_{ei\sigma_2}^* y_{j\mu\sigma_2} y_{je\sigma_1} \right] \quad (3.20)$$

where, $\tilde{D}_0 = \tilde{D}_0(m_{F_i^0}, m_{F_j^0}, m_{\sigma_1}, m_{\sigma_2})$ and $D_0 = D_0(m_{F_i^0}, m_{F_j^0}, m_{\sigma_1}, m_{\sigma_2})$. Here, $\sigma_{1,2}$ ranges over Δ_1^+ and Δ_2^+ .

The term $B_{(c)}^{\text{quartet}}$ corresponds to the contribution of the charged fermions and it reads

$$e^2 B_{(c)}^{\text{quartet}} = \frac{1}{16\pi^2} \sum_{i,j=1}^3 \sum_{\sigma_1, \sigma_2} \frac{\tilde{D}_0}{2} y_{ei\sigma_1}^* y_{i\mu\sigma_2} y_{ej\sigma_2}^* y_{je\sigma_1} \quad (3.21)$$

Here, $\tilde{D}_0 = \tilde{D}_0(m_{F_i^\pm}, m_{F_j^\pm}, m_{\sigma_1}, m_{\sigma_2})$ and $\sigma_{1,2}$ ranges over Δ^{++} , S , A .

3.3 $\mu - e$ conversion in nuclei

The conversion rate, normalized by the muon capture rate is [27, 64–66]

$$\begin{aligned} \text{CR}(\mu - e, \text{Nucleus}) = \frac{p_e E_e m_\mu^3 G_F^2 \alpha_{em}^3 Z_{eff}^4 F_p^2}{8\pi^2 Z \Gamma_{\text{capt}}} \left\{ |(Z + N)(g_{LV}^{(0)} + g_{LS}^{(0)}) + (Z - N)(g_{LV}^{(1)} + g_{LS}^{(1)})|^2 \right. \\ \left. + |(Z + N)(g_{RV}^{(0)} + g_{RS}^{(0)}) + (Z - N)(g_{RV}^{(1)} + g_{RS}^{(1)})|^2 \right\} \quad (3.22) \end{aligned}$$

Here, Z and N are the number of protons and neutrons in the nucleus, Z_{eff} is the effective atomic charge, F_p is the nuclear matrix element and Γ_{capt} represents the total muon capture rate. p_e and E_e are the momentum and energy of the electron

(taken as $\sim m_\mu$ in the numerical evaluation). $g_{XK}^{(0)}$ and $g_{XK}^{(1)}$ ($X = L, R$ and $K = V, S$) in the above expression are given as

$$\begin{aligned} g_{XK}^{(0)} &= \frac{1}{2} \sum_{q=u,d,s} (g_{XK(q)} G_K^{(q,p)} + g_{XK(q)} G_K^{(q,n)}) \\ g_{XK}^{(1)} &= \frac{1}{2} \sum_{q=u,d,s} (g_{XK(q)} G_K^{(q,p)} - g_{XK(q)} G_K^{(q,n)}) \end{aligned} \quad (3.23)$$

$g_{XK(q)}$ are the couplings in the effective Lagrangian describing $\mu - e$ conversion,

$$\mathcal{L}_{eff} = -\frac{G_F}{\sqrt{2}} \sum_q \{ [g_{LS(q)} \bar{e}_L \mu_R + g_{RS(q)} \bar{e}_R \mu_L] \bar{q} q + [g_{LV(q)} \bar{e}_L \gamma^\mu \mu_L + g_{RV(q)} \bar{e}_R \gamma^\mu \mu_R] \bar{q} \gamma_\mu q \} \quad (3.24)$$

$G^{(q,p)}, G^{(q,n)}$ are the numerical factors that arise when quark matrix elements are replaced by the nucleon matrix elements,

$$\langle p | \bar{q} \Gamma_K q | p \rangle = G_K^{(q,p)} \bar{p} \Gamma_K p, \quad \langle n | \bar{q} \Gamma_K q | n \rangle = G_K^{(q,n)} \bar{n} \Gamma_K n \quad (3.25)$$

For the inert scalar model, the $\mu - e$ conversion rate receives the γ , Z and Higgs penguin contributions. In γ and Z penguin diagrams, $\bar{q} q$ ($q=u,d,s$) line is attached to γ line of $\mu e \gamma$ vertex and Z boson line of $\mu e Z$ vertex respectively. It doesn't receive any box contribution because there is no coupling between inert scalars and quarks because of the Z_2 symmetry. Moreover, Higgs penguin contribution is small compared to γ and Z penguin diagrams because of small Yukawa couplings thus neglected in our numerical analysis. The relevant effective coupling for the conversion in the inert scalar model is

$$\begin{aligned} g_{LV(q)} &= g_{LV(q)}^\gamma + g_{LV(q)}^Z \\ g_{RV(q)} &= g_{LV(q)}|_{L \leftrightarrow R} \\ g_{LS(q)} &\approx 0, \quad g_{RS(q)} \approx 0 \end{aligned}$$

The relevant couplings are

$$g_{LV(q)}^\gamma = \frac{\sqrt{2}}{G_F} e^2 Q_q (A_{ND} - A_D) \quad (3.26)$$

$$g_{LV(q)}^Z = -\frac{\sqrt{2}}{G_F} \frac{g_L^q + g_R^q}{2} \frac{F_Z}{m_Z^2} \quad (3.27)$$

Here Q_q is the electric charge of the quarks and Z boson couplings to the quarks are

$$g_L^q = \frac{g}{\cos \theta_W} (T_3^q - Q_q \sin^2 \theta_W), \quad g_R^q = -\frac{g}{\cos \theta_W} Q_q \sin^2 \theta_W \quad (3.28)$$

Also the relevant numerical factors for nucleon matrix elements are

$$G_V^{(u,p)} = G_V^{(d,n)} = 2, \quad G_V^{(d,p)} = G_V^{(u,n)} = 1 \quad (3.29)$$

4 Results and Discussion

In this section we have presented our numerical results and discussed the phenomenological implications of those results for larger scalar multiplets. But before presenting the results, we have listed all the constraints regarding dark matter and collider searches so that our analysis can focus on parameter space for where both inert doublet and quartet models are viable.

There are two possible dark matter (DM) candidates in the inert scalar models. In the doublet model they are the lightest right handed neutrino, N_1 and the lightest neutral scalar, S of the doublet. On the other hand, in the quartet model the neutral component of the lightest fermion triplet, F_1^0 and the lightest neutral scalar, S of the quartet can play the dark matter role. In both cases fermionic and scalar DM give rise to different phenomenology. In this preliminary study of comparing different LFV rates in inert scalar models, we have chosen the scalar as the DM particle and used the constraints associated with it in our analysis.

4.1 Constraints and parameter space

4.1.1 Collider constraints

For the doublet scalar, the collider searches have put the following mass constraints, $m_{C^+} \gtrsim 100$ GeV, $m_S \gtrsim 65 - 80$ GeV and $m_A \gtrsim 140$ GeV [17–21]. Although there hasn't been any collider studies on the quartet, one can recast the constraints of the doublet case onto the quartet. As the quartet scalar has the cascade decay channel, we can expect multilepton final states along with missing transverse energy similar to doublet. Therefore, the mass constraints for quartet, compatible with bounds on electroweak precision observable [67], are $m_{\Delta_{1,2}}, m_{\Delta^{++}} \gtrsim 100$ GeV, $m_S \gtrsim 65 - 80$ GeV and $m_A \gtrsim 140$ GeV. Considering S as the DM also set the mass hierarchy in quartet components: $m_S < m_{\Delta_1^+} < m_{\Delta^{++}} < m_{\Delta_2^+} < m_A$. In contrast, the scalar masses in the TeV scale for both doublet and quartet are fairly unconstrained.

In the case of fermions, the masses of RH neutrino in the doublet case are not constrained by current collider data. In contrast, fermion triplet of the quartet case, having gauge interaction, will have an accessible collider signature. In [68] the mass of the charged component of the triplet is excluded up to 270 GeV with 8 TeV 20.3 fb⁻¹ LHC data. Moreover, in [69] it was shown that the projected reach for 14 TeV collider with 3 ab⁻¹ luminosity (High luminosity LHC phase) would be $M_F \lesssim 500$ GeV, for (future) 100 TeV pp collider with 3 ab⁻¹ luminosity in mono-jet searches, $M_F \lesssim 1.3$ TeV, and with 30 ab⁻¹ luminosity, $M_F \lesssim 1.7$ TeV.

4.1.2 DM Constraints

The dark matter density of the universe measured by Planck collaboration is $\Omega_{DM} h^2 = 0.1196 \pm 0.0031$ (68% CL) [70]. In the inert scalar model, there are two viable mass region of scalar DM. They are the low mass region ($m_S < m_W$) and the high mass

region ($m_S \gg m_W$). The low mass DM region of doublet model has been extensively studied. In addition, same region for DM in the quartet was addressed in [22] where it was shown that it is harder to achieve low mass dark matter with correct relic density compared to the doublet because, for most of the parameter space, bounds on electroweak T parameter sets the mass of single charged component, Δ_1^+ close to the DM mass and therefore it is not only in tension with collider bounds but also opens up coannihilation channel and leads to a sub-dominant DM in the universe.

In the high mass region of the doublet, as shown in [71], the DM mass starts from a lower bound of $m_0 = 534 \pm 25$ GeV (where the thermal freeze-out only happens through the gauge interaction) to 20 TeV if the higgs-scalar coupling, $\lambda_S \lesssim 2\pi$. The maximal mass splitting compatible with correct relic density, are

$$|m_A - m_S| \lesssim 16.9 \text{ GeV}, \quad |m_{C^+} - m_S| \lesssim 14.6 \text{ GeV} \quad (4.1)$$

when $m_S \sim O(5 \text{ TeV})$.

In the case of high mass region for the quartet, we have used FeynRules [72] to generate the model files for MicrOMEGAS [73] and have found out that the DM mass starts from a lower bound of 2.46 TeV (freeze out only through gauge interaction)² to upper bound of 14 TeV set again by $\lambda_S \lesssim 2\pi$ bound. In this case, the mass splitting between the DM and other components are

$$\begin{aligned} |m_A - m_S| &\lesssim 16 \text{ GeV}, \quad |m_{\Delta_2^+} - m_S| \lesssim 14 \text{ GeV} \\ |m_{\Delta^{++}} - m_S| &\lesssim 12 \text{ GeV}, \quad |m_{\Delta_1^+} - m_S| \lesssim 1 \text{ GeV} \end{aligned} \quad (4.2)$$

when $m_S \sim O(5 \text{ TeV})$. figure 2 presents the $m_S - \lambda_S$ plane with allowed region for both doublet and quartet scalar DM by the relic density and direct detection bound [74]. Here, λ_S is effective coupling of S to Higgs field as can be seen in eq. (2.6). From figure 2, we can see that there is an overlapping region on the plane where doublet and quartet DM satisfy the constraints simultaneously.

The γ coupling which controls the mass splitting between scalar (DM) and pseudoscalar component, has the range $\gamma \in [10^{-9}, 2.7]$ for the doublet and $\gamma \in [10^{-9}, 1.36]$ to be consistent with the relic density. But it gets another constraint from bounds on DM inelastic scattering with nuclei. If the typical velocity of a DM particle, χ is $\beta_\chi c \sim 220 \text{ km/sec}$, the inelastic scattering is kinematically forbidden if the splitting Δ_χ between DM and the next to lightest component is larger,

$$\Delta_\chi > \frac{\beta_\chi^2 m_\chi M_{\text{nucleus}}}{2(m_\chi + M_{\text{nucleus}})}$$

Therefore one would require, $\gamma \gtrsim 10^{-5}$ to kinematically forbid the inelastic scattering of scalar DM with O(TeV) mass. As the inelastic scattering is mediated by the

²without considering the Sommerfeld enhancement

exchange of Z boson and the scattering cross section is in the order of $10^{-40} - 10^{-39} \text{ cm}^2$, which is much larger than the direct detection bounds, the allowed range of γ for doublet and quartet DM are $\gamma \in [10^{-5}, 2.7]$ and $\gamma \in [10^{-5}, 1.36]$, respectively.

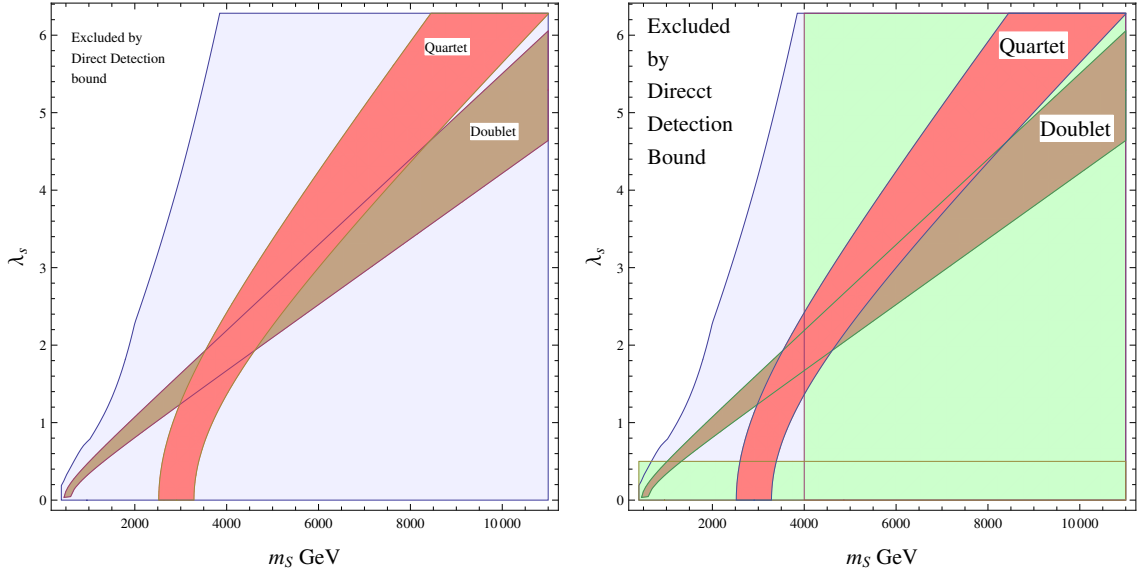


Figure 2. Correlation between the mass of the DM, m_S and the effective coupling between the Higgs and the DM, λ_S for the doublet and quartet case. Here, the white region is excluded by the direct detection bound from the LUX collaboration [74]. The left figure represents the correlation without taking into account the Sommerfeld enhancement in the thermal freeze-out. In the right figure, for the green shaded region, Sommerfeld enhancement is not negligible.

4.1.3 Gamma ray constraints and Sommerfeld enhancement

Compared to the collider searches and DM direct detection experiments, indirect detection can set limits on the inert scalar DM at the TeV mass range because of a certain enhancement in the annihilation cross sections.

At small relative velocity, two particles interacting via a long range force receive non-perturbative enhancement in the interaction cross section which is known as Sommerfeld enhancement [75]. When the mass of the DM is much larger than the mass of W and Z bosons, the electroweak interaction effectively behaves like a long range force, thus pair annihilation cross sections of the DM also receive Sommerfeld enhancements as pointed in [76–78]. At present, as the relative velocity of DM is about 10^{-3} , Sommerfeld enhancement significantly boosts the indirect detection signals, specially the gamma rays produced from the DM annihilation and put stringent constraint on the DM in the light of the experimental observations. In fact it was shown for the case of wino dark matter [81, 82] and minimal DM models (5-plet

fermion and 7-plet scalar with zero hypercharge) [83–85] (and references therein) that they are highly constrained to be the dominant DM of the universe by the experimental limits on gamma ray spectrum due to the Sommerfeld enhancement in the pair annihilation cross section.

Having electroweak charge, the heavy DM component of the inert scalar multiplet is also expected to have enhancements in both weak and scalar interactions. Although the full treatment of Sommerfeld enhancement for inert scalar model is beyond the scope of this work, following [79, 80], we introduce the dimensionless parameters to curve out the regions of the parameter space where the enhancement takes place and where the enhancement is negligible. The parameters are, $\epsilon_{v_{\text{DM}}} = (v_{\text{DM}}/c)/\alpha$, $\epsilon_\phi = (m_\phi/m_{\text{DM}})/\alpha$ and $\epsilon_\delta = \sqrt{2\delta/m_{\text{DM}}}/\alpha$. Here v_{DM} is the relative velocity of the DM particle, m_ϕ is the mass of the gauge boson carrying the force, δ is the mass splitting between the DM and the next to lightest charged component of the multiplet and α is the coupling constant of the relevant interaction. It was shown in [80] that the Sommerfeld enhancement is relevant if $\epsilon_{v_{\text{DM}}}, \epsilon_\phi, \epsilon_\delta \lesssim 1$. On the other hand, it is negligible for the region of parameter space where any of $\epsilon_{v_{\text{DM}}}, \epsilon_\phi, \epsilon_\delta > 1$.

In the case of the minimal DM models, the processes contributing to the gamma spectrum from DM annihilation are, $\text{DM DM} \rightarrow W^+W^-, ZZ$ where the decay and fragmentation of W and Z pairs produce secondary photons and $\text{DM DM} \rightarrow \gamma\gamma, \gamma Z$ producing line spectrum of mono energetic photons. The Sommerfeld enhancement takes place when the DM-DM two particle state changes into DM^+DM^- two particle state, where DM^\pm is the next to lightest charged state, by exchanging W boson and subsequently charged states annihilate. For the minimal DM case, the DM and next to lightest charged state is almost degenerate (only loop induced mass splitting of the $O(100)$ MeV), so $\epsilon_\delta < 1$ for $\alpha_w = 1/30$ and TeV scale DM and one can have Sommerfeld enhanced annihilation cross section. On the other hand, for the inert scalar models, the following terms in the scalar potential

$$V \supset \beta \Phi^\dagger \tau^a \Phi \Delta^\dagger T^a \Delta + \gamma [(\Phi^T \epsilon \tau^a \Phi)(\Delta^T C T^a \Delta)^\dagger + h.c] \quad (4.3)$$

can split the DM component and other charged component of the multiplet after electroweak symmetry breaking. For example, for quartet, when $m_S = 3$ TeV and $\delta = m_{\Delta_1^+} - m_S = 1.5$ GeV, ϵ_δ is 1.001. In addition, from figure 3, we can see that the bounds on electroweak precision observables allow maximum mass splitting to be 8.78 GeV and corresponding ϵ_δ is 2.46. Therefore for such mass splitting, according to [80], the Sommerfeld enhancement can be negligible in the inert scalar models.

Moreover, Sommerfeld enhancement also affects the thermal freeze-out of the minimal DM as pointed out in [47, 48]. Such enhancement is also expected in the case of inert scalar DM. But if the thermal freeze-out happens after the electroweak phase transition, one can introduce enough mass splitting so that $\epsilon_\delta > 1$. In fact, $\delta = 1.5$ GeV is compatible with the observed DM relic density of the universe with $m_S = 3$ TeV for both doublet and quartet scalar DM. On the other hand, if freeze-out

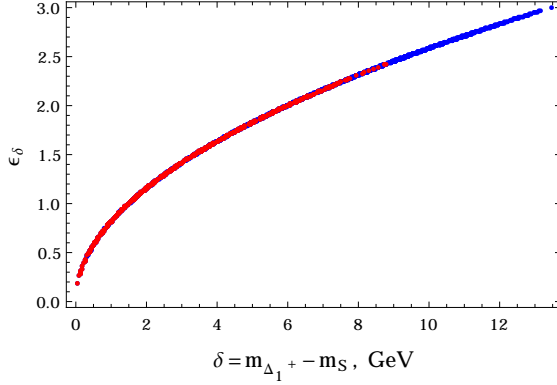


Figure 3. ϵ_δ vs $\delta = m_{\Delta_1^+} - m_S$ for DM mass, $m_S = 3000$ GeV in the quartet. Here, blue points are allowed by stability conditions on the scalar potential and perturbative limits on scalar couplings. Red points are allowed by the bounds on electroweak precision observables.

temperature, T_F is larger than the critical temperature of electroweak phase transition, T_{PT} , the thermal freeze-out takes place before the electroweak phase transition and there will not be any mass splitting to suppress the enhancement. Therefore thermal DM scenario of inert scalar DM will be different than that of the broken phase. But the value of the critical temperature of the electroweak phase transition depends on the model, order of the transition and its dynamics (see for example [86, 87]). For this reason, we consider the range, $T_{PT} = 100 - 200$ GeV for the transition temperature. Now if $x_f = M_{DM}/T_F \sim 20$, we see that for $m_{DM} > 4$ TeV, freeze out takes place in the unbroken phase and will involve Sommerfeld enhanced annihilation cross-sections.

On the other hand, for $M_{DM} < 4$ TeV, the DM freezes out in the broken phase. So one can introduce the enough mass splitting, $\delta \sim 1.5$ GeV between the DM and next to lightest charged state to suppress the enhancement in the annihilation cross sections.

For the inert scalar multiplets, apart from gauge interactions, the DM interacting via higgs exchange is also expected to have enhancement. In this case, the Yukawa potential V_{sc} experienced by the DM is

$$V_{sc}(r) = \alpha_{sc} \frac{e^{-m_h r}}{r} \quad \text{with} \quad \alpha_{sc} = \frac{\lambda_S^2}{4\pi} \frac{v^2}{m_S^2} \quad (4.4)$$

For example, if $m_S = 1$ TeV and $\lambda_S = \pi$, $\alpha_{sc} = 0.047$ so $\epsilon_\phi = 2.6$ for the Higgs exchange, therefore the enhancement is generally not important for scalar interaction with the DM mass at TeV range.

In summary, although the DM with mass at TeV range in the inert scalar model is expected to have Sommerfeld enhancement in the gauge interactions and can have significantly enhanced indirect detection signal, there is a small common region of

parameter space for doublet and quartet as seen from figure 2 (right) where one can have enough mass splitting to suppress the Sommerfeld enhancement in the inert scalar models and such mass splitting is compatible with the observed DM relic density. Therefore in the subsequent analysis, we only focus that small region of parameter space with benchmark point, $m_S = 3$ TeV and $\delta = 1.5$ GeV and have left the complete analysis of Sommerfeld enhancement in the inert quartet case for future work [90].

4.1.4 Scalar coupling and LFV rates with scalar DM

There is a correlation between the γ coupling of the scalar sector and the rate of LFV processes when R in eq. (2.1) is a real orthogonal matrix. As we can see from eq. (2.15) and eq. (2.17) that the smaller value of γ leads to smaller value of the loop factor Λ_i and thus neutrino mass. This in turn increases the Yukawa coupling, as in eq. (2.20), and becomes inconsistent with perturbativity bound eq. (2.21) when γ is very small. On the other hand, large value of γ implies larger separation in m_S and m_A and also in $m_{\Delta_1^+}$ and $m_{\Delta_2^+}$, thus larger value of Λ_i and in this case the value of Yukawa coupling is reduced. In figure 4 (left), We have illustrated this by comparing $\text{Br}(\mu \rightarrow e\gamma)$ for $\gamma = 10^{-9}$ and 10^{-5} respectively. We can see that for $\gamma = 10^{-5}$, the rate has become out of reach for current and future experiments. Therefore in the case of real R matrix, $\gamma \sim O(10^{-9})$ leads to appreciable LFV rates. However we have seen in Sec. 4.1.2 that as one would require, $\gamma \gtrsim 10^{-5}$ to kinematically forbid the inelastic scattering of scalar DM with O(TeV) mass so considering only real R will lead to negligible rates of LFV processes.

On the other hand, in the case of complex R , such correlation between γ and the rates of LFV processes is not straightforward because the size of Yukawa coupling also depends on the imaginary part of the complex angles in R . For simplicity, we have added an imaginary part, $\text{Im}(z)$, in three angles of R and in figure 4 (right), we can see that, despite having $\gamma = 10^{-5}$, $\text{Br}(\mu \rightarrow e\gamma)$ become comparable to the current bound with increasing values of $\text{Im}(z)$. Again perturbativity of the Yukawa coupling typically put upper bound on $\text{Im}(z)$ of $O(3 - 5)$. Therefore, one can have viable scalar DM in both doublet and quartet models where $\xi > 1$ with appreciable LFV rates by tuning the Imaginary part of complex angles in R .

4.1.5 Viable parameter space

The parameter space for the model consists of $\{M_0, \alpha, \beta, \gamma\}$ of the scalar sector and $\{M_{N(F)}, y_{i\alpha}\}$ of the fermionic sector. Here M_N and M_F are the masses of RH neutrino and real fermion triplet (as the components of the triplet are degenerate at tree level) respectively.

The focus of this preliminary study is the comparison among different LFV rates in doublet and quartet model with scalar DM. At first, from figure 2, as an exemplary point, we have chosen the mass of scalar DM to be $m_S = 3$ TeV with $\lambda_S = 1.3$ in

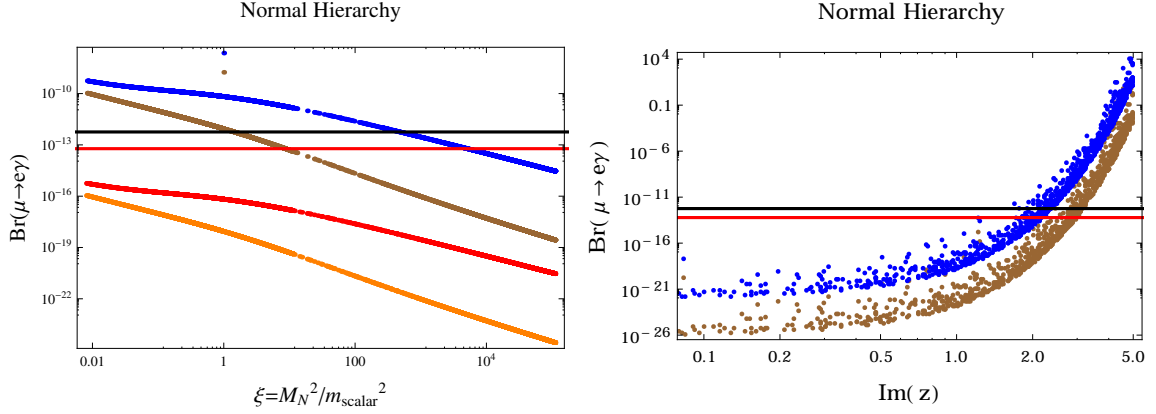


Figure 4. Left figure presents the dependence of the rate of LFV processes on the γ when the R is a real matrix. Here we have considered only $\text{Br}(\mu \rightarrow e\gamma)$ for illustration. The brown and blue represents the rate in the doublet and quartet cases respectively for $\gamma = 10^{-9}$. On the other hand, the orange and red points represents the rate in the doublet and quartet cases respectively for $\gamma = 10^{-5}$. Right figure presents the correlation of the rate in doublet (brown points) and quartet (blue points) with imaginary part of the complex angle, $\text{Im}(z)$, when we consider complex R matrix. Here The scalar mass is fixed at $m_{\text{scalar}} = 3000$ GeV and $\gamma = 10^{-5}$. The black horizontal line is the current bound 5.7×10^{-13} and red line is projected bound 6×10^{-14} .

the $m_S - \lambda_S$ plane so that scalar DM is viable both in doublet and quartet model. Moreover, γ is set to be 10^{-5} to be consistent with bounds from DM direct detection. As the components of the scalar multiplet are almost degenerate apart from the very small splitting induced by non zero γ . Therefore we set the average mass of the scalar components at $m_{\text{scalar}} = 3$ TeV.

There are two sets of fermion mass range we have considered in our analysis. For the comparison of LFV rates with the variation of fermion masses both in doublet and quartet model, we have evaluate them in two sets, namely, i) where $\xi = M_{N(F)}^2 / m_{\text{scalar}}^2 < 1$ so that the scalar component ceases to be the DM and ii) where $\xi > 1$ where the scalar component is the DM. We have varied the masses of RH neutrinos and the fermion triplet within the range, $M_{N(F)} \in (270 \text{ GeV}, 30 \text{ TeV})$ which encompasses both sets mentioned above. 270 GeV is taken as the lower limit of fermion mass as triplet fermion is excluded up to that mass in collider searches. Also such range is considered to see how the LFV rates vary with the mass of the fermion in addition to the DM aspects of inert scalar model.

We have used the experimental values of low energy neutrino parameters, U_{PMNS} , $\Delta m_{\text{solar}}^2$ and Δm_{atm}^2 as the input in eq. (2.1) for Yukawa couplings. For both normal and inverted hierarchies, we could only vary the lowest neutrino mass, m_{ν_1} , the Dirac phase, δ and Majorana phases, α_ν , β_ν and three complex angles, z_1 , z_2 , z_3 of, R . In our numerical analysis, as an simplification, the lowest neutrino mass is set to $m_\nu = 1$

meV, $\delta \in [0, 2\pi]$, $\alpha = \beta = 0$ and common imaginary part in $z_i = \theta_i + i \text{Im}(z_i)$, $\text{Im}(z)$ with the range $(0, 5)$.

Summarizing, our input parameters in the numerical scans are $\{M_0, \alpha, \beta, \gamma, M_N = M_F = \tilde{M}, m_{\nu_1}, \delta, \alpha_\nu, \beta_\nu, \theta_1, \theta_2, \theta_3, \text{Im}(z)\}$ satisfying all the constraints mentioned above. Therefore, we can compare the LFV rates in both models for common viable point in the parameter space.

4.2 LFV processes

In the inert scalar models with scalar DM in the high mass regime, there is no direct correlation between the Yukawa couplings and DM properties. Also we have seen that the real matrix R and $\gamma \gtrsim 10^{-5}$ (scalar DM direct detection constraint) give rise to small Yukawa couplings which in turn lead to LFV rates beyond the reach of current and future experiments as seen in figure 4 (left). But the size of the Yukawa coupling can be enhanced by varying the imaginary part of complex angles of R without substantially affecting the phenomenology of the scalar DM and despite having $\gamma \gtrsim 10^{-5}$, we can easily obtain the LFV rates within the experimental range.

So first we have compared the rates of $\mu \rightarrow e\gamma$, $\mu \rightarrow ee\bar{e}$ and $\mu - e$ conversion rate with $\gamma = 10^{-5}$ and the real R matrix by varying the fermion masses for the doublet and quartet models. Then we vary $\text{Im}(z)$ within its constrained limits and determine the region allowed by current and future bounds on the rates of these three LFV processes for both doublet and quartet cases. Also when $\xi > 1$, we have our scalar dark matter in both doublet and quartet models.

4.2.1 $\text{Br}(\mu \rightarrow e\gamma)$

Due to the excellent bound put by the MEG collaboration [33, 34], $\mu \rightarrow e\gamma$ is one of the most well studied LFV processes. figure 5 shows the comparison of this process between the doublet (brown points) and the quartet (blue points) scalar. We can see that the quartet contribution to $\mu \rightarrow e\gamma$ is larger than that of the doublet. For the same parameter point, in the quartet case, additional charged and neutral scalar ($\Delta_1^\pm, \Delta_2^\pm, \Delta^{\pm\pm}, S$ and A) and fermion states (F_i^0 and F_i^\pm) enter in the loop compared to single charged scalar (C^\pm) and neutral fermion state (N_i) in the doublet case and as the contributions of extra states are additive, the rate has increased in the quartet case than that of the doublet. From figure 5 we can see that $\text{Br}(\nu \rightarrow e\gamma)$ is larger for the quartet than the doublet for both $\xi < 1$ and $\xi > 1$ (where the doublet and quartet scalars are the DM).

4.2.2 $\text{Br}(\mu \rightarrow ee\bar{e})$

In $\mu \rightarrow ee\bar{e}$, the dominant contributions are coming from γ -penguin and Box diagrams. The Higgs penguin diagram is suppressed by the small electron Yukawa coupling. The Z penguin contribution is small because of the cancellation that takes place between C_{24} and B_1 terms in eq. (3.12) and also between the same terms in eq.

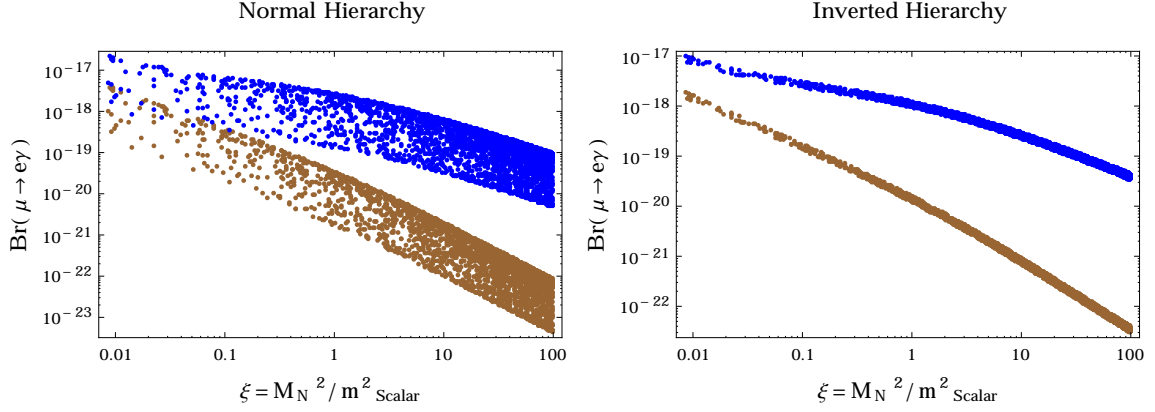


Figure 5. Correlation between $\xi = M_{N(F)}^2/m_{\text{scalar}}^2$ and $\text{Br}(\mu \rightarrow e\gamma)$ for doublet (brown points) and quartet (blue points) with normal (left fig.) and inverted (right fig.) hierarchy for light neutrino mass. Here we have taken $M_{N(F)}$ to be degenerate, random Dirac phase δ and random real matrix R . Also we have set Majorana phases α_ν and β_ν to be zero in this case. The scalar mass is fixed at $m_{\text{scalar}} = 3000$ GeV. Also $\gamma = 10^{-5}$ and light neutrino mass, $m_{\nu_1} = 1$ meV.

(3.15) when $m_{\sigma_1} = m_{\sigma_2}$. Moreover, similar cancellation takes place between the first two lines and third line of eq. (3.16) due to the specific relations among the couplings in front of the vertices. Therefore Z penguin contribution is also small in $\mu \rightarrow ee\bar{e}$ for both inert doublet and quartet case. Also note that the Z contribution in the quartet case is relatively bigger than that in the doublet because in the quartet m_{σ_1} and m_{σ_2} are not exactly equal when $\sigma_1 \neq \sigma_2$. Hence one receives larger Z-penguin contribution in the quartet compared to the doublet. Still this contribution is numerically not significant if we compare it with γ penguin diagram or box diagram contributions. From figure 6, we can see that $\text{Br}(\mu \rightarrow ee\bar{e})$ is larger for quartet (blue points) compared to the doublet (brown points) for both $\xi < 1$ and $\xi > 1$ cases.

4.2.3 $\mu - e$ conversion rate

Another prominent LFV process currently under investigation is the $\mu - e$ conversion in nuclei. Here we have calculated the $\mu - e$ conversion rate for Ti and Au nuclei in the inert model with doublet and quartet. From figure 7, we can see that the $\mu - e$ conversion rate is larger for the quartet (blue points) compared to the doublet (brown points). The dip occurs in the doublet contribution at $\xi = 1$ because at that value, the dipole contribution A_D^{doublet} and the non-dipole contribution A_{ND}^{doublet} are equal as they are coming from single γ penguin diagram involving charged scalar C^\pm and neutral fermion N_i and eq. (3.26) indicates that the effective coupling is zero for doublet at that point. On the other hand, for quartet case A_D^{quartet} and A_{ND}^{quartet} at $\xi = 1$ are different because more than one charged scalar contribute to the γ penguin diagrams. Again we can see from figure 7 that the conversion rate is larger for the

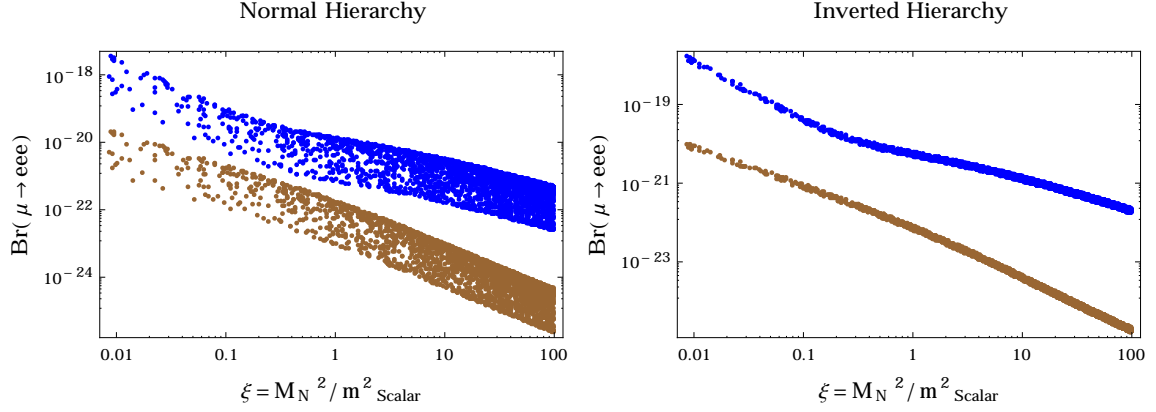


Figure 6. Correlation between $\xi = M_{N(F)}^2/m_{\text{scalar}}^2$ and $\text{Br}(\mu \rightarrow ee\bar{e})$ for doublet (brown points) and quartet (blue points) with normal (left fig.) and inverted (right fig.) hierarchy for light neutrino mass. Here we have taken same input parameters as in $\text{Br}(\mu \rightarrow e\gamma)$.

quartet than that for the doublet for both $\xi < 1$ and $\xi > 1$ cases. We have not included the figure for $\mu - e$ conversion rate in Au nuclei as it is similar to figure 7.

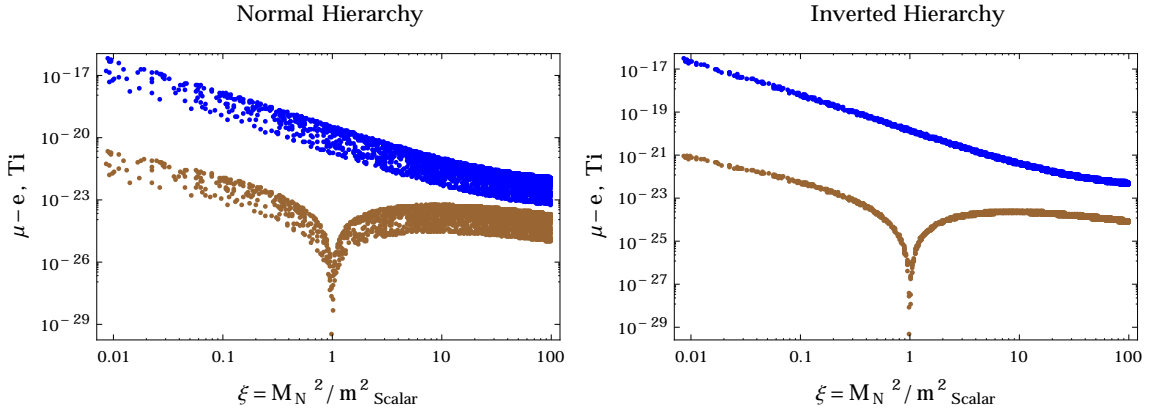


Figure 7. Correlation between $\xi = M_{N(F)}^2/m_{\text{scalar}}^2$ and $\mu - e$ conversion rate for Ti nucleus. for doublet (brown points) and quartet (blue points) with normal (left fig.) and inverted (right fig.) hierarchy for light neutrino mass. Here we have taken same input parameters as in $\text{Br}(\mu \rightarrow e\gamma)$.

4.2.4 LFV rates in the doublet and quartet

As expected, the LFV rates seen in figure 5, 6 and 7 are very small for real R and $\gamma = 10^{-5}$. The rates will reduce even more if we increase γ . Still the rates are larger for the quartet compared to the doublet for $\xi < 1$ and $\xi > 1$ case where scalar is treated as the DM candidate. Now we increase the value of $\text{Im}(z)$ and calculate the LFV rates with increasing values of \tilde{M} .

From figure 8, we can see that LFV rates in the quartet are more constrained than those in the doublet for common parameter space satisfying all the restrictions

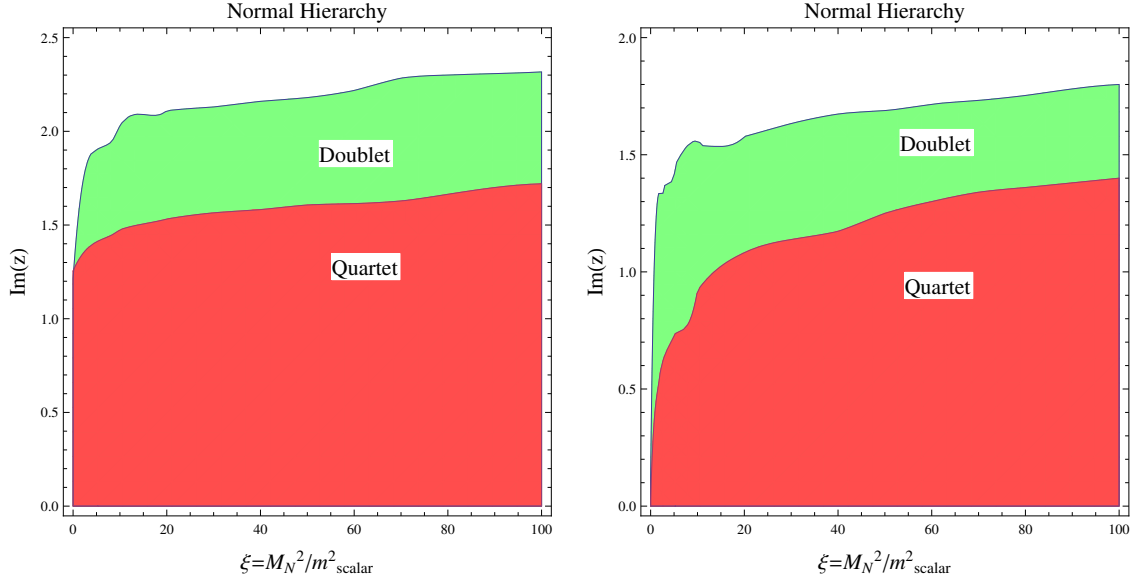


Figure 8. The $\xi - \text{Im}(z)$ plane for degenerate $M_{N(F)}$, random Dirac phase δ , zero Majorana phases $\alpha_\nu = \beta_\nu = 0$ and light neutrino mass, $m_{\nu_1} = 1$ meV. The scalar mass is $m_{\text{scalar}} = 3000$ GeV with $\gamma = 10^{-5}$. In (left), the current bounds are imposed: $\text{Br}(\mu \rightarrow e\gamma) \lesssim 5.9 \times 10^{-13}$, $\text{Br}(\mu \rightarrow ee\bar{e}) \lesssim 1 \times 10^{-12}$ and $\mu - e$ conversion rate for Ti $\lesssim 4.3 \times 10^{-12}$. In (right), the future sensitivity are considered: $\text{Br}(\mu \rightarrow e\gamma) \lesssim 6.4 \times 10^{-14}$, $\text{Br}(\mu \rightarrow ee\bar{e}) \lesssim 1 \times 10^{-16}$ and $\mu - e$ conversion rate for Ti $\lesssim 10^{-18}$.

of Sec. 4.1. The allowed regions on $\xi - \text{Im}(z)$ plane are reduced further for both doublet and quartet models if one imposes the sensitivity of future lepton flavor violating experiments. The case for inverted hierarchy shows similar pattern so we have only presented results regarding normal hierarchy.

5 Conclusions

The scotogenic model is a well studied neutrino mass model and lepton flavor violation is one of its important phenomenological aspects. In this study we present the comparison among different LFV processes in the inert doublet and the quartet model, taking into account the current experimental limits and future sensitivity. There are two possible dark matter candidates in the inert scalar models: scalar and fermionic DM. In this study we have considered scalar DM and evaluated LFV rates for common parameter space subjected to collider bounds, DM constraints for doublet and quartet model and low-energy neutrino parameters. Our results are summarized as follows

- $\text{Br}(\mu \rightarrow e\gamma)$, $\text{Br}(\mu \rightarrow ee\bar{e})$ and $\mu - e$ conversion rates in nuclei in the quartet model are larger than those in the doublet model for the same parameter

space as seen from figure 5, 6 and 7. In the case of higher scalar representation more particles enter into the loops and their contributions are additive in the LFV processes. Therefore we can have larger rates of different LFV processes compared to the lower scalar representation. From figure 8, we can see that, LFV processes in higher scalar representation are more constrained by the current and near-future experiments. In addition, this phenomenological result is complementary to the appearance of low scale Landau pole for higher representations [22, 88, 89].

- There is no significant deviation from figure 5-8 for non-degenerate right handed neutrinos and real fermion triplets. In the case of large hierarchy, $m_{N_3} \gg m_{N_{1,2}}$, the dominant contribution comes from only the lightest generation.

We would like to emphasize here that the conclusion of our preliminary study is applicable to the inert scalar models where scalar DM is considered. But there is much room for an improved analysis. For example, in the case of fermionic DM, the DM constraints will be different and will have different viable parameter set for the LFV rate comparison. Also one needs to study the DM properties and viability of a common parameter space where $\xi \sim 1$. Therefore, further quantitative analysis of the fermionic DM aspects in the quartet model will be presented in a future publication [90]. Furthermore, similar analysis can be carried out for $\tau \rightarrow \mu\gamma$, $\tau \rightarrow ee\bar{e}$, $\tau \rightarrow \mu\mu\bar{\mu}$ in the inert scalar models to probe the flavor structure of the Yukawa sector and to have better constraints on the higher scalar representation in the light of experimental limits.

Acknowledgements

We would like to thank Avelino Vicente for stimulating discussion. T.A.C is grateful to Fernando Quevedo, Bobby Acharya and the HECAP section of ICTP for the support and the hospitality where the initial part of this work has been carried out. We are also indebted to the Referee for the constructive report, for which, the result and presentation of our study has been substantially improved.

A Scalar masses

A.1 Inert Doublet

The mass spectrum for the inert doublet in our parametrization eq. (2.2) is,

$$\begin{aligned} m_S^2 &= M_0^2 + \frac{1}{2} \left(\alpha + \frac{1}{4}\beta + \gamma \right) v^2 \\ m_A^2 &= M_0^2 + \frac{1}{2} \left(\alpha + \frac{1}{4}\beta - \gamma \right) v^2 \\ m_C^2 &= M_0^2 + \frac{1}{2} \left(\alpha + \frac{1}{4}\beta \right) v^2 \end{aligned} \quad (\text{A.1})$$

A.2 Inert Quartet

In the inert quartet case, the γ term, apart from splitting S and A , also mixes two single charged components of the quartet. According to eq. (2.9), the mass matrix for single charged fields in (Δ^+, Δ'^+) basis is

$$M_+^2 = \begin{pmatrix} M_0^2 + \frac{1}{2}(\alpha - \frac{1}{4}\beta)v^2 & \frac{\sqrt{3}}{2}\gamma v^2 \\ \frac{\sqrt{3}}{2}\gamma v^2 & M_0^2 + \frac{1}{2}(\alpha + \frac{3}{4}\beta)v^2 \end{pmatrix} \quad (\text{A.2})$$

Diagonalizing the mass matrix, we have mass eigenstates for single charged fields, $\Delta_1^+ = \Delta^+ \cos \theta + \Delta'^+ \sin \theta$, $\Delta_2^+ = -\Delta^+ \sin \theta + \Delta'^+ \cos \theta$ with $\tan 2\theta = -\frac{2\sqrt{3}\gamma}{\beta}$.

Therefore the mass spectrum of the quartet is

$$\begin{aligned} m_{S(A)}^2 &= M_0^2 + \frac{1}{2} \left(\alpha + \frac{1}{4}\beta \mp 2\gamma \right) v^2 \\ m_{\Delta_{++}}^2 &= M_0^2 + \frac{1}{2} \left(\alpha - \frac{3}{4}\beta \right) v^2 \\ m_{\Delta_1^+(\Delta_2^+)}^2 &= M_0^2 + \frac{1}{2} \left(\alpha + \frac{1}{2}\beta \mp \frac{1}{2}\sqrt{\beta^2 + 12\gamma^2} \right) v^2 \end{aligned} \quad (\text{A.3})$$

Because of the mixing between two single charged states, the mass relation is

$$m_S^2 + m_A^2 = m_{\Delta_1^+}^2 + m_{\Delta_2^+}^2 \quad (\text{A.4})$$

B Loop functions

The loop functions relevant for the dipole and non-dipole form factors from $\mu e \gamma$ vertex are

$$F^{(n)}(x) = \frac{1 - 6x + 3x^2 + 2x^3 - 6x^2 \ln x}{6(1-x)^4} \quad (\text{B.1})$$

$$F^{(c)}(x) = \frac{2 + 3x - 6x^2 + x^3 + 6x \ln x}{6(1-x)^4} \quad (\text{B.2})$$

$$G^{(n)}(x) = \frac{2 - 9x + 18x^2 - 11x^3 + 6x^3 \ln x}{6(1-x)^4} \quad (\text{B.3})$$

$$G^{(c)}(x) = \frac{16 - 45x + 36x^2 - 7x^3 + 6(2 - 3x) \ln x}{6(1-x)^4} \quad (\text{B.4})$$

In the following we collect the Passarino-Veltman loop functions.

$$B_1(m_1, m_2) = -\frac{1}{2} - \frac{m_1^4 - m_2^4 + 2m_1^4 \ln \frac{m_2^2}{m_1^2}}{4(m_1^2 - m_2^2)^2} + \frac{1}{2} \ln \frac{m_2^2}{\mu^2} \quad (\text{B.5})$$

$$C_0(m_1, m_2, m_3) = \frac{m_2^2(m_1^2 - m_3^2) \ln \frac{m_2^2}{m_1^2} - (m_1^2 - m_2^2)m_3^2 \ln \frac{m_3^2}{m_1^2}}{(m_1^2 - m_2^2)(m_1^2 - m_3^2)(m_2^2 - m_3^2)} \quad (\text{B.6})$$

$$C_{24}(m_1, m_2, m_3) = \frac{1}{8(m_1^2 - m_2^2)(m_1^2 - m_3^2)(m_2^2 - m_3^2)} \left[-2(m_1^2 + m_2^2)m_3^4 \ln \frac{m_3^2}{m_1^2} - (m_3^2 - m_1^2) \right. \\ \left. \left(2m_2^4 \ln \frac{m_2^2}{m_1^2} + (m_1^2 - m_2^2)(m_2^2 - m_3^2) \left(2 \ln \frac{m_1^2}{\mu^2} - 3 \right) \right) \right] \quad (\text{B.7})$$

$$\tilde{D}_0(m_1, m_2, m_3, m_4) = \frac{m_2^4 \ln \frac{m_2^2}{m_1^2}}{(m_2^2 - m_1^2)(m_2^2 - m_3^2)(m_2^2 - m_4^2)} - \frac{m_3^4 \ln \frac{m_3^2}{m_1^2}}{(m_3^2 - m_1^2)(m_3^2 - m_2^2)(m_3^2 - m_4^2)} \\ - \frac{m_4^4 \ln \frac{m_4^2}{m_1^2}}{(m_4^2 - m_1^2)(m_4^2 - m_2^2)(m_4^2 - m_3^2)} \quad (\text{B.8})$$

$$D_0(m_1, m_2, m_3, m_4) = \frac{m_2^2 \ln \frac{m_2^2}{m_1^2}}{(m_2^2 - m_1^2)(m_2^2 - m_3^2)(m_2^2 - m_4^2)} - \frac{m_3^2 \ln \frac{m_3^2}{m_1^2}}{(m_3^2 - m_1^2)(m_3^2 - m_2^2)(m_3^2 - m_4^2)} \\ - \frac{m_4^2 \ln \frac{m_4^2}{m_1^2}}{(m_4^2 - m_1^2)(m_4^2 - m_2^2)(m_4^2 - m_3^2)} \quad (\text{B.9})$$

C $\mu e\gamma$ vertex, μeZ vertex and box diagrams

C.1 $\mu e\gamma$ vertex

Here we present in figure 9 the Feynman diagrams of one-loop contributions of the doublet and quartet to the $\mu e\gamma$ vertex.

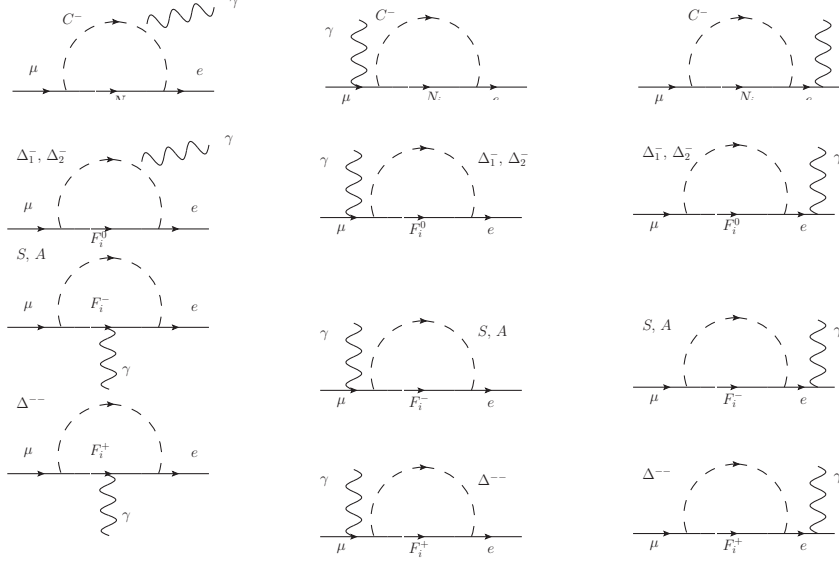
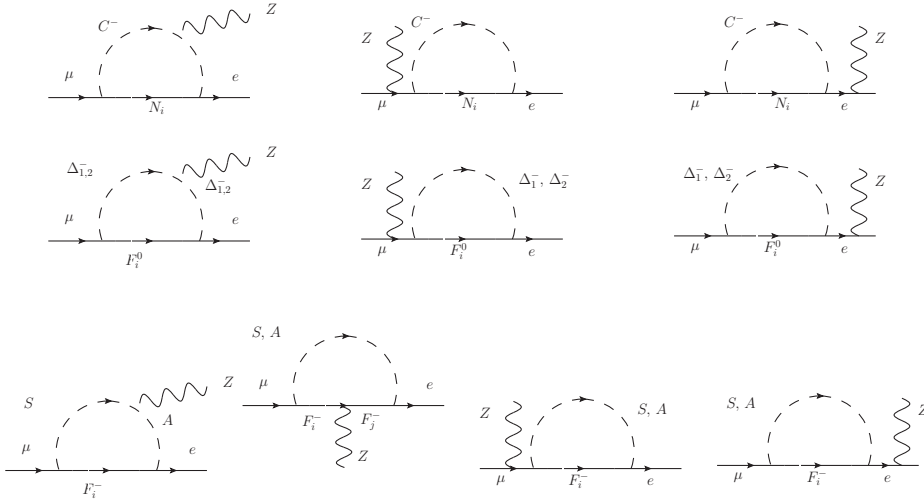


Figure 9. $\mu e\gamma$ vertex and the self energy diagrams of the external fermions for the doublet (first row) and the quartet cases (second to fourth rows).

C.2 μeZ vertex

We present in figure 10 the Feynman diagrams of one-loop contributions of the doublet and the quartet to the μeZ vertex.



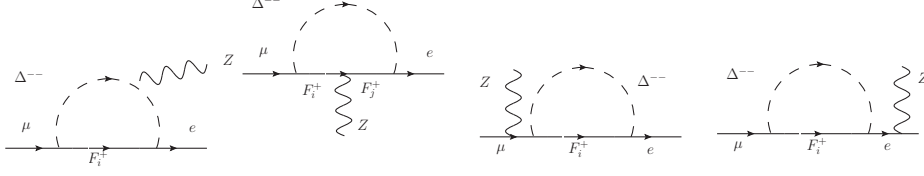


Figure 10. $\mu e Z$ vertex and the self energy diagrams of the external fermions for the doublet (first row) and the quartet cases (second to fourth rows).

C.3 Box diagrams

The box diagrams for the doublet and the quartet cases are given in figure 11,

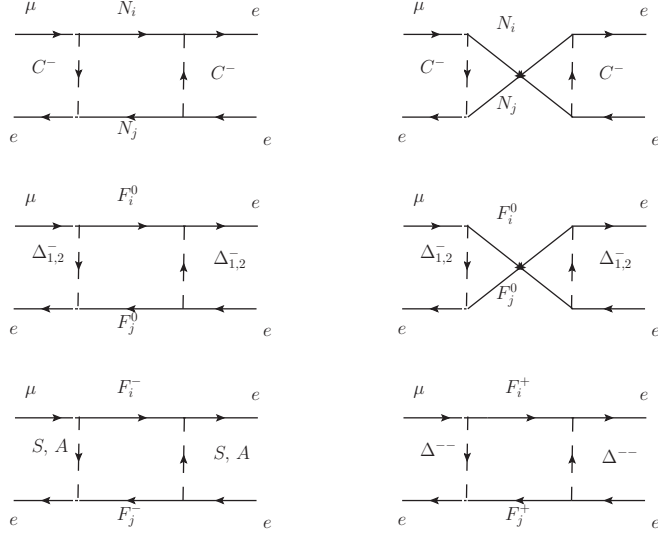


Figure 11. Box diagrams for the doublet (first row) and the quartet (second and third rows).

References

- [1] E. Ma, Phys. Rev. D **73**, 077301 (2006) [hep-ph/0601225].
- [2] N. G. Deshpande and E. Ma, Phys. Rev. D **18**, 2574 (1978).
- [3] L. Lopez Honorez, E. Nezri, J. F. Oliver and M. H. G. Tytgat, JCAP **0702**, 028 (2007) [hep-ph/0612275].
- [4] E. M. Dolle and S. Su, Phys. Rev. D **80**, 055012 (2009) [arXiv:0906.1609 [hep-ph]].

- [5] L. Lopez Honorez and C. E. Yaguna, JCAP **1101**, 002 (2011) [arXiv:1011.1411 [hep-ph]].
- [6] P. Agrawal, E. M. Dolle and C. A. Krenke, Phys. Rev. D **79**, 015015 (2009) [arXiv:0811.1798 [hep-ph]].
- [7] S. Andreas, M. H. G. Tytgat and Q. Swillens, JCAP **0904**, 004 (2009) [arXiv:0901.1750 [hep-ph]].
- [8] E. Nezri, M. H. G. Tytgat and G. Vertongen, JCAP **0904**, 014 (2009) [arXiv:0901.2556 [hep-ph]].
- [9] Q. -H. Cao, E. Ma and G. Rajasekaran, Phys. Rev. D **76**, 095011 (2007) [arXiv:0708.2939 [hep-ph]].
- [10] H. Martinez, A. Melfo, F. Nesti, G. Senjanović, Phys. Rev. Lett. **106**, 191802 (2011). [arXiv:1101.3796 [hep-ph]].
- [11] A. Melfo, M. Nemevšek, F. Nesti, G. Senjanović, Y. Zhang, Phys. Rev. **D84** (2011) 034009. [arXiv:1105.4611 [hep-ph]].
- [12] T. A. Chowdhury, M. Nemevšek, G. Senjanović and Y. Zhang, JCAP **1202**, 029 (2012) [arXiv:1110.5334 [hep-ph]].
- [13] D. Borah and J. M. Cline, Phys. Rev. D **86**, 055001 (2012) [arXiv:1204.4722 [hep-ph]].
- [14] G. Gil, P. Chankowski and M. Krawczyk, Phys. Lett. B **717**, 396 (2012) [arXiv:1207.0084 [hep-ph]].
- [15] J. M. Cline and K. Kainulainen, Phys. Rev. D **87**, 071701 (2013) [arXiv:1302.2614 [hep-ph]].
- [16] A. Ahriche, G. Faisel, S. Y. Ho, S. Nasri and J. Tandean, Phys. Rev. D **92** (2015) 3, 035020 [arXiv:1501.06605 [hep-ph]].
- [17] E. Lundstrom, M. Gustafsson and J. Edsjo, Phys. Rev. D **79**, 035013 (2009) [arXiv:0810.3924 [hep-ph]].
- [18] E. Dolle, X. Miao, S. Su and B. Thomas, Phys. Rev. D **81**, 035003 (2010) [arXiv:0909.3094 [hep-ph]].
- [19] M. Gustafsson, S. Rydbeck, L. Lopez-Honorez and E. Lundstrom, Phys. Rev. D **86**, 075019 (2012) [arXiv:1206.6316 [hep-ph]].
- [20] M. Aoki, S. Kanemura and H. Yokoya, Phys. Lett. B **725**, 302 (2013) [arXiv:1303.6191 [hep-ph]].
- [21] G. Belanger, B. Dumont, A. Goudelis, B. Herrmann, S. Kraml and D. Sengupta, arXiv:1503.07367 [hep-ph].
- [22] S. S. AbdusSalam and T. A. Chowdhury, JCAP **1405**, 026 (2014) [arXiv:1310.8152 [hep-ph]].
- [23] J. Kubo, E. Ma and D. Suematsu, Phys. Lett. B **642** (2006) 18 [hep-ph/0604114].

- [24] D. Aristizabal Sierra, J. Kubo, D. Restrepo, D. Suematsu and O. Zapata, Phys. Rev. D **79** (2009) 013011 [arXiv:0808.3340 [hep-ph]].
- [25] D. Suematsu, T. Toma and T. Yoshida, Phys. Rev. D **79** (2009) 093004 [arXiv:0903.0287 [hep-ph]].
- [26] A. Adulpravitchai, M. Lindner and A. Merle, Phys. Rev. D **80** (2009) 055031 [arXiv:0907.2147 [hep-ph]].
- [27] T. Toma and A. Vicente, JHEP **1401** (2014) 160 [arXiv:1312.2840, arXiv:1312.2840 [hep-ph]].
- [28] A. Vicente and C. E. Yaguna, JHEP **1502** (2015) 144 [arXiv:1412.2545 [hep-ph]].
- [29] E. Ma and D. Suematsu, Mod. Phys. Lett. A **24** (2009) 583 [arXiv:0809.0942 [hep-ph]].
- [30] S. S. C. Law and K. L. McDonald, JHEP **1309** (2013) 092 [arXiv:1305.6467 [hep-ph]].
- [31] B. Ren, K. Tsumura and X. G. He, Phys. Rev. D **84** (2011) 073004 [arXiv:1107.5879 [hep-ph]].
- [32] A. Ahriche, K. L. McDonald, S. Nasri and T. Toma, Phys. Lett. B **746** (2015) 430 [arXiv:1504.05755 [hep-ph]].
- [33] J. Adam *et al.* [MEG Collaboration], Phys. Rev. Lett. **107** (2011) 171801 [arXiv:1107.5547 [hep-ex]].
- [34] J. Adam *et al.* [MEG Collaboration], Phys. Rev. Lett. **110** (2013) 201801 [arXiv:1303.0754 [hep-ex]].
- [35] A. M. Baldini, F. Cei, C. Cerri, S. Dussoni, L. Galli, M. Grassi, D. Nicolo and F. Raffaelli *et al.*, arXiv:1301.7225 [physics.ins-det].
- [36] U. Bellgardt *et al.* [SINDRUM Collaboration], Nucl. Phys. B **299** (1988) 1.
- [37] A. Blondel, A. Bravar, M. Pohl, S. Bachmann, N. Berger, M. Kiehn, A. Schoning and D. Wiedner *et al.*, arXiv:1301.6113 [physics.ins-det].
- [38] W. H. Bertl *et al.* [SINDRUM II Collaboration], Eur. Phys. J. C **47** (2006) 337.
- [39] C. Dohmen *et al.* [SINDRUM II Collaboration], Phys. Lett. B **317** (1993) 631.
- [40] D. Glenzinski [Mu2e Collaboration], AIP Conf. Proc. **1222** (2010) 383.
- [41] L. Bartoszek *et al.* [Mu2e Collaboration], arXiv:1501.05241 [physics.ins-det].
- [42] H. Natori [DeeMe Collaboration], Nucl. Phys. Proc. Suppl. **248-250** (2014) 52.
- [43] Y. Kuno [COMET Collaboration], PTEP **2013** (2013) 022C01.
- [44] Y. Kuno, Nucl. Phys. Proc. Suppl. **149** (2005) 376.
- [45] R. J. Barlow, Nucl. Phys. Proc. Suppl. **218** (2011) 44.
- [46] M. Cirelli, N. Fornengo and A. Strumia, Nucl. Phys. B **753** (2006) 178 [hep-ph/0512090].

- [47] M. Cirelli, A. Strumia and M. Tamburini, Nucl. Phys. B **787**, 152 (2007) [arXiv:0706.4071 [hep-ph]].
- [48] M. Cirelli and A. Strumia, New J. Phys. **11**, 105005 (2009) [arXiv:0903.3381 [hep-ph]].
- [49] J. A. Casas and A. Ibarra, Nucl. Phys. B **618** (2001) 171 [hep-ph/0103065].
- [50] J. A. Casas, J. M. Moreno, N. Rius, R. Ruiz de Austri and B. Zaldivar, JHEP **1103** (2011) 034 [arXiv:1010.5751 [hep-ph]].
- [51] J. Heeck, Phys. Rev. D **86**, 093023 (2012) [arXiv:1207.5521 [hep-ph]].
- [52] T. P. Cheng and L. F. Li, Phys. Rev. Lett. **38** (1977) 381.
- [53] T. P. Cheng and L. F. Li, Phys. Rev. D **16** (1977) 1425.
- [54] T. P. Cheng and L. F. Li, Phys. Rev. Lett. **45** (1980) 1908.
- [55] E. Ma and A. Pramudita, Phys. Rev. D **24** (1981) 1410.
- [56] C. S. Lim and T. Inami, Prog. Theor. Phys. **67** (1982) 1569.
- [57] A. Ilakovac and A. Pilaftsis, Nucl. Phys. B **437** (1995) 491 [hep-ph/9403398].
- [58] A. Blum and A. Merle, Phys. Rev. D **77** (2008) 076005 [arXiv:0709.3294 [hep-ph]].
- [59] J. Hisano, T. Moroi, K. Tobe and M. Yamaguchi, Phys. Rev. D **53** (1996) 2442 [hep-ph/9510309].
- [60] E. Arganda and M. J. Herrero, Phys. Rev. D **73** (2006) 055003 [hep-ph/0510405].
- [61] M. E. Krauss, W. Porod, F. Staub, A. Abada, A. Vicente and C. Weiland, Phys. Rev. D **90**, no. 1, 013008 (2014) [arXiv:1312.5318 [hep-ph]].
- [62] A. Abada, M. E. Krauss, W. Porod, F. Staub, A. Vicente and C. Weiland, JHEP **1411** (2014) 048 [arXiv:1408.0138 [hep-ph]].
- [63] E. Arganda and M. J. Herrero, arXiv:1403.6161 [hep-ph].
- [64] R. Kitano, M. Koike and Y. Okada, Phys. Rev. D **66** (2002) 096002 [Phys. Rev. D **76** (2007) 059902] [hep-ph/0203110].
- [65] E. Arganda, M. J. Herrero and A. M. Teixeira, JHEP **0710** (2007) 104 [arXiv:0707.2955 [hep-ph]].
- [66] A. Crivellin, M. Hoferichter and M. Procura, Phys. Rev. D **89** (2014) 093024 [arXiv:1404.7134 [hep-ph]].
- [67] J. Beringer *et al.* [Particle Data Group Collaboration], Phys. Rev. D **86**, 010001 (2012).
- [68] G. Aad *et al.* [ATLAS Collaboration], Phys. Rev. D **88** (2013) 11, 112006 [arXiv:1310.3675 [hep-ex]].
- [69] M. Cirelli, F. Sala and M. Taoso, JHEP **1410** (2014) 033 [JHEP **1501** (2015) 041] [arXiv:1407.7058 [hep-ph]].

- [70] P. A. R. Ade *et al.* [Planck Collaboration], *Astron. Astrophys.* **571**, A16 (2014) [arXiv:1303.5076 [astro-ph.CO]].
- [71] T. Hambye, F.-S. Ling, L. Lopez Honorez and J. Rocher, *JHEP* **0907** (2009) 090 [*JHEP* **1005** (2010) 066] [arXiv:0903.4010 [hep-ph]].
- [72] A. Alloul, N. D. Christensen, C. Degrande, C. Duhr and B. Fuks, *Comput. Phys. Commun.* **185** (2014) 2250 [arXiv:1310.1921 [hep-ph]].
- [73] G. Belanger, F. Boudjema, A. Pukhov and A. Semenov, *Comput. Phys. Commun.* **185** (2014) 960 [arXiv:1305.0237 [hep-ph]].
- [74] D. S. Akerib *et al.* [LUX Collaboration], *Phys. Rev. Lett.* **112** (2014) 091303 [arXiv:1310.8214 [astro-ph.CO]].
- [75] A. Sommerfeld, *Ann. Phys.* **11**, 257 (1931)
- [76] J. Hisano, S. Matsumoto and M. M. Nojiri, *Phys. Rev. Lett.* **92**, 031303 (2004) [hep-ph/0307216].
- [77] J. Hisano, S. Matsumoto, M. M. Nojiri and O. Saito, *Phys. Rev. D* **71**, 063528 (2005) [hep-ph/0412403].
- [78] J. Hisano, S. Matsumoto, O. Saito and M. Senami, *Phys. Rev. D* **73**, 055004 (2006) [hep-ph/0511118].
- [79] N. Arkani-Hamed, D. P. Finkbeiner, T. R. Slatyer and N. Weiner, *Phys. Rev. D* **79** (2009) 015014 [arXiv:0810.0713 [hep-ph]].
- [80] T. R. Slatyer, *JCAP* **1002** (2010) 028 [arXiv:0910.5713 [hep-ph]].
- [81] J. Fan and M. Reece, *JHEP* **1310**, 124 (2013) [arXiv:1307.4400 [hep-ph]].
- [82] T. Cohen, M. Lisanti, A. Pierce and T. R. Slatyer, *JCAP* **1310**, 061 (2013) [arXiv:1307.4082].
- [83] M. Cirelli, T. Hambye, P. Panci, F. Sala and M. Taoso, *JCAP* **1510**, no. 10, 026 (2015) [arXiv:1507.05519 [hep-ph]].
- [84] C. Garcia-Cely, A. Ibarra, A. S. Lamperstorfer and M. H. G. Tytgat, *JCAP* **1510**, no. 10, 058 (2015) [arXiv:1507.05536 [hep-ph]].
- [85] M. Aoki, T. Toma and A. Vicente, *JCAP* **1509**, 063 (2015) [arXiv:1507.01591 [hep-ph]].
- [86] M. Quiros, hep-ph/9901312.
- [87] D. E. Morrissey and M. J. Ramsey-Musolf, *New J. Phys.* **14**, 125003 (2012) [arXiv:1206.2942 [hep-ph]].
- [88] L. Di Luzio, R. Grober, J. F. Kamenik and M. Nardecchia, arXiv:1504.00359 [hep-ph].
- [89] Y. Hamada, K. Kawana and K. Tsumura, arXiv:1505.01721 [hep-ph].
- [90] T. A. Chowdhury and S. Nasri, *in preparation*.